Chaotic diffusion across a magnetic field in a model of electrostatic turbulent plasma

Marco Pettini

Osservatorio Astrofisico di Arcetri and Istituto Nazionale di Fisica Nucleare, Sezione di Firenze,
Largo E. Fermi 5, 50125 Firenze, Italy

Angelo Vulpiani

Dipartimento di Fisica, Università di Roma I, Piazzale Aldo Moro 2, 00185 Roma, Italy

Jacques H. Misguich

Association EURATOM-Commissariat à l'Energie Atomique sur la Fusion, Département de Recherches sur la Fusion Contrôlée,
Centre d'Etudes Nucléaires de Cadarache, 13108 Saint-Paul-lez-Durance, Cédex, France

Michel De Leener, John Orban, and Radu Balescu

Association EURATOM-Etat Belge and Faculté des Sciences, Université Libre de Bruxelles, Cassella Postale 231,
Campus Plaine, 1050 Bruxelles, Belgium

(Received 25 June 1987)

We have investigated the particle-guiding center motion (across a strong magnetic field) caused by a time-dependent electrostatic field. Two different nonlinear Hamiltonian systems of 1.5 degrees of freedom have been used. The Hamiltonian is proportional to the electrostatic potential, which is defined through its spatial Fourier spectrum in two dimensions. A k^{-3} power-law spectrum (k is the wave vector) and random-phase shifts have been chosen to model the spatial dependence of the electrostatic drift-wave turbulence observed in several tokamaks. The equations of motion have been solved numerically. When the average electric field amplitude is larger than a threshold value, the particle trajectories become chaotic at large scale and a diffusion across the magnetic field sets in. The diffusion coefficient D has been measured for different values of the average electric field amplitude A. The classical (quasilinear) scaling has been found at small A, $D \propto A^2$, while a transition to the Bohm scaling is found at higher amplitudes, $D \propto A$. A recently proposed theoretical treatment of the same problem has been applied to our models and the theoretical predictions have been compared to the results of numerical simulations. For relative diffusion, the theoretical prediction of the so-called "clump effect" has been well confirmed by numerical simulations. Theory and simulation are in qualitative agreement for the dependence of D on A, but some quantitative discrepancies exist; their nature is discussed.

I. INTRODUCTION

At present, the major obstacle to the realization of controlled thermonuclear fusion in closed magnetic configuration devices (tokamaks) is commonly attributed to the existence of anomalous energy losses due to particle and energy transport across the confining magnetic field. These energy losses are higher than those predicted by the neoclassical theory of collisional transport and they result in an enhancement of electron thermal conduction.[1]

Plasma microturbulence is generally believed[2] to be at the origin of anomalous transport; in fact, the strong fluctuations of electric (or magnetic) field on spatial scales much smaller than the plasma radius—i.e., strong field gradient—result in an enhancement of the diffusion, as if the collision frequency had grown. Among the different possibilities of generating plasma microturbulence, much interest has been addressed to electrostatic fluctuations of low frequencies, driven by pressure gradients (drift-wave turbulence).

Even if such electrostatic fluctuations have been ob-

served in all the tokamaks where appropriate measurements have been carried on,[3,4] there is as yet little conclusive evidence that these low-frequency, microscopic fluctuations are indeed the cause of observed anomalous transport in tokamaks.[2] Moreover, several recent results[5] have clearly shown the inadequacy of the available empirical transport models. Therefore a deeper understanding of the diffusion properties of charged particles in turbulent electromagnetic fields is urgent. The assessment of the actual importance of these fluctuations for the anomalous transport is an open and important problem.

Beyond the existing empirical models for tokamak transport, as far as the theoretical background of turbulent plasma transport is concerned, any theory of plasma turbulence yielding expressions for the correlations of the various fluctuating quantities also yields transport coefficients. Many such turbulence theories have been proposed but no attempt to review them is made here. We just want to recall that when the level of turbulence is low, nonlinearities are treated by perturbation techniques (weak-turbulence theory[6]) and the transport coefficients depend on the energy level of the fluctuating fields; thus

for small fluctuation levels (in the so-called quasilinear approximation) the diffusion coefficient scales quadratically with the average electric field amplitude.

For drift-wave turbulence even with a fluctuation level of a few percent the perturbative approach is no longer valid and the plasma must be considered as strongly nonlinear, i.e., strongly turbulent. In this case renormalization techniques have been developed,[7] with the assumption of incoherent fluctuations resulting from strong nonlinear coupling. In the limit of strong turbulence the scaling of the diffusion coefficient with the average electric field becomes linear.

In any case, the renormalization prescriptions rely on simple closure assumptions which are rather familiar in fluid turbulence. In fact, the commonly used[8] second-cumulant approximation for the closure problem is essentially a quasinormal approximation, very similar to the direct interaction approximation (DIA) introduced by Kraichnan[9] for fluid turbulence. Another approach in the incoherent fluctuations picture is known as "clump" theory and has been proposed by Dupree,[10] and Kadomtsev and Pogutse[11] (see also Refs. 12 and 13).

In recent years a great deal of work has been done on nonlinear dynamical systems in the hope that turbulent systems, fluids or plasmas, could ultimately be described with the aid of few relevant degrees of freedom. A close interaction in many topics between theoretical plasma physics and classical mechanics has proved to be very fruitful.

So a new approach to the problem of turbulent diffusion has been recently tried. The diffusion (transport) properties are investigated in nonlinear Hamiltonian systems obtained, for instance, from the equation of motion

$$\frac{d\mathbf{x}(t)}{dt} = \frac{c}{|\mathbf{B}|^2}\mathbf{E}[\mathbf{x}(t),t]\times\mathbf{B} \ . \tag{1}$$

Usually the approximation of this approach is to leave aside the self-consistent particle-field interaction problem, and to study the behavior of test particles in given fields $\mathbf{E}[\mathbf{x}(t),t]$.

The equation above is obtained in the limit of an electric field varying at low frequencies, as compared to the electron and ion gyrofrequencies Ω_e and Ω_i, and in the presence of a strong magnetic field $\mathbf{B}$ so that the fast component of charged particle motion (The Larmor gyration) can be averaged in the so-called guiding-center approximation.

Recently, such a model has been studied in the case of two drift waves.[14] Even this very simplified model displays an interesting behavior. The conditions on wave frequencies to obtain stochastic particle motion, and hence diffusion, have been established together with the dependence of the diffusion coefficient on the field fluctuation amplitude and some insight into the details of particle transport has been gained. On the same model a very interesting theoretical work has been carried on;[15] conditions for the destruction of robust elliptic fixed points (with the onset of global stochasticity) have been analyzed in detail to determine the conditions for the diffusion approximation to be valid.

The aim of the present paper is to report the results obtained with a nonlinear dynamical model where some of the spectral properties of the turbulence—measured in tokamaks—are taken into account (even if in a still very idealized way). The comparison of these results with the theoretical predictions of a recent turbulent diffusion theory[16] is also presented; this was, in fact, among the original motivations of this work. Preliminary results were given in Ref. 17.

Passing from the simplest system of waves which can yield stochastic particle motion (i.e., a two-wave model) to a system where a power-law $\mathbf{k}$ spectrum is considered, many results change. The most important difference is that we have found a quadratic dependence of the diffusion coefficient on the r.m.s. electric fields $\tilde{E}$ for "small" $\tilde{E}$, and a linear dependence for "large" $\tilde{E}$ ($\tilde{E}=\langle\,|\mathbf{E}\,|^2\rangle^{1/2}$ and $\langle\,\cdots\,\rangle$ stands for spatial average).

Both of these regimes are predicted by the theory;[16] they may be identified with the quasilinear and Bohm diffusion regimes respectively. On the contrary, the two-wave model yields a much slower increase of D in terms of $\tilde{E}$.[10]

We have also observed the so-called clump effect[8,10–13,16] in the case of guiding centers; this effect shows up in the relative diffusion of close particles and is consistent with an exponential separation of neighboring orbits. A relevant result is that a simple scaling law is found for

$$\langle\,\delta r^2(t)\,\rangle = \langle\,[\mathbf{x}^{(1)}(t)-\mathbf{x}^{(2)}(t)]^2\,\rangle$$

in a wide range of turbulent amplitudes $\tilde{E}$, that is,

$$\langle\,\delta r^2(t)\,\rangle = F[tD(\tilde{E})] \ ,$$

a property predicted by the theory[16] in the range of moderate amplitudes.

In Sec. II we introduce the model. In Sec. III the numerical methods and particle trajectories are described. In Sec. IV we report the results for absolute and relative diffusion, Kolmogorov entropy and other statistical properties and trajectories. Section V is devoted to a slightly different model introduced to test the "structural stability" of our results. In Sec. VI the comparison between theoretical and numerical results is done for absolute and relative diffusion. Conclusions are reported in Sec. VII.

II. DESCRIPTION OF THE MODEL

We consider a plasma in a strong, constant, and uniform magnetic field $\mathbf{B}=B\hat{\mathbf{z}}$, where $\hat{\mathbf{z}}$ is the unit vector in the z direction. The electric field and the guiding-center velocities have only x and y components. The observed turbulent spectrum $S(\mathbf{k},\omega)$ of electric field fluctuations is modeled in terms of a given electrostatic field $\mathbf{E}(\mathbf{x},t)=-\nabla\Phi(\mathbf{x},t)$ with

$$\Phi(\mathbf{x},t)=\sum_{\mathbf{k}}\Phi_{\mathbf{k}}\sin[\mathbf{k}\cdot\mathbf{x}+\varphi_{\mathbf{k}}-\omega(\mathbf{k})t] \ , \tag{2}$$

where $\varphi_{\mathbf{k}}$ are random phases and the $\Phi_{\mathbf{k}}$ decrease as a given function of $\mathbf{k}$, in agreement with experimental data.

In general, the frequency is $\mathbf{k}$ dependent according to a dispersion law $\mathcal{F}[\mathbf{k},\omega(\mathbf{k})]=0$, but for simplicity we have

taken $\omega(\mathbf{k})=\omega_0$, a constant. This could be the case for Langmuir waves, but in the case of drift-wave turbulence this has to be considered as a simple approximation, necessary to make numerical simulation feasible.

Finally the wave-number spectrum $S(\mathbf{k})$ is chosen to have a simple power-law dependence so that it reproduces the k^{-3} subrange energy spectrum which has been observed in drift-wave turbulence.[4] Equation (1) for guiding centers is

$$\frac{d}{dt}\begin{bmatrix}x\\y\end{bmatrix}=\frac{c}{B}\begin{bmatrix}E_y(x,y,t)\\-E_x(x,y,t)\end{bmatrix}=\frac{c}{B}\begin{bmatrix}-\partial_y\Phi\\\partial_x\Phi\end{bmatrix}.\qquad(3)$$

Note that the system (3) is a nonautonomous Hamiltonian system in which the coordinates x and y play the role of canonical coordinates and the time-dependent Hamiltonian is

$$H(x,y,t)=\frac{c}{B}\Phi(x,y,t)\ .\qquad(4)$$

Thus the physical space (x,y) is also the phase space of the system.

In this section we consider the following explicit form of the electrostatic potential (model I):

$$\Phi(x,y,t)=\frac{a_{\mathrm{I}}}{2\pi}\sum_{\substack{m=1\\n^2+m^2\le N^2}}^{N}\sum_{n=1}^{N}\frac{1}{(n^2+m^2)^{3/2}}$$

$$\times\sin\left[\frac{2\pi}{L}(nx+my)\right.$$

$$\left.+\varphi_{nm}-\omega_0 t\right]\ ,\qquad(5)$$

where the phases φ_{nm} are chosen at random in a uniform distribution on the interval $(0,2\pi)$; only those modes (n,m) with $n^2+m^2\le N^2$ are taken into account.

This potential has periodicity lengths equal to L in both x and y directions; in other words, the potential configuration of the unit square $(0,L)\times(0,L)\in\mathbb{R}^2$, at any given time, is indefinitely repeated in space. In general

$$\mathbf{k}=\begin{bmatrix}n\\m\end{bmatrix}k_0\equiv\begin{bmatrix}n\\m\end{bmatrix}\frac{2\pi}{L}\ ;$$

the smallest wave vector in (5) is thus

$$\mathbf{k}_{\min}=N_0 k_0\begin{bmatrix}1\\1\end{bmatrix}$$

(with $N_0=1$ in this section). We have

$$L=N_0\lambda_{\max}\equiv N_0 2\pi/k_{\min}=N\lambda_{\min}\ ,\qquad(6)$$

where we introduced by definition $k_{\min}=N_0 k_0$. The width ν of the $\mathbf{k}$ spectrum is given by $\nu=k_{\min}/k_{\max}=N_0/N$.

The frequency ω_0 can be thought of as an effective average frequency for drift waves; even if this is a limitation of the model (we still have a coherent variation in

time of the potential), the chaotic dynamics makes the Lagrangian field (i.e., the field felt by the particles along their trajectories) incoherently fluctuating. This fact is well known from many examples of smooth and nonchaotic Eulerian fields[18] where chaotic Lagrangian fields are obtained.

We report in Fig. 1 a computer-made drawing representing the equipotential curves of a generic realization of the turbulent electric field. A picture of the potential is shown at $t=0$. The first property of our model of a turbulent potential field is that it is strongly fluctuating in time. Actually, the eddies of Fig. 1 are rapidly modified in the course of time: where a vortex was initially present, an open line appears, and so on.

This behavior is not simply explained by the propagation of the structure (see below). The effect of the random phases in producing eddies that are irregular in space is also clearly important. Note that the strong decay law of the Fourier coefficients of the field (k^{-3}) tends to hide the small-scale contributions.

Two peculiar properties of our model, anisotropy and propagation, have also been observed: each image of the potential field shows an elongated structure of the eddies; moreover by superposing the images obtained at different times a slight propagation in the $y=x$ direction is found. However, this propagation can easily be proved not to perturb the diffusive motion of the guiding centers. The two properties of anisotropy and propagation are easily understood analytically. Restricting ourselves to the most simplified case of an electric potential given only by a dominant mode $(n=m=1)$,

$$\Phi_{11}=\frac{a_{\mathrm{I}}}{2\pi}2^{-3/2}\sin\left[\frac{2\pi}{L}(x+y)+\varphi_{11}-\omega_0 t\right]\ ,\qquad(7)$$

we immediately realize that at any given time the maxima
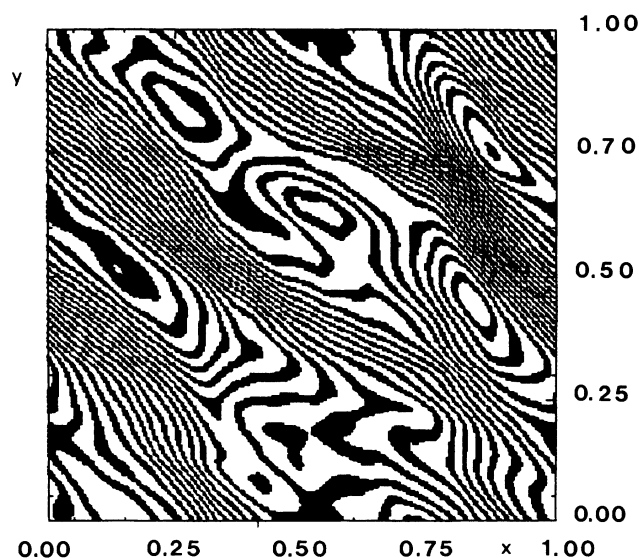
FIG. 1. Equipotential curves [Eq. (5)] of the turbulent electric field (for $t=0$). The thickness of lines is proportional to the local flatness of the potential.

and minima of the sine are located on the lines $y = -x + \text{const}$. As the amplitudes Φ_{nm} are rapidly decreasing functions of n and m, the structure of (7) is essentially preserved also in the case of many waves ($N \gg 1$). Moreover, it is obvious that, with the potential (7), any given line $y = x + c$ (where a maximum or a minimum is attained) moves in time with the phase velocity; this is the reason why we say that our model is a "propagative" one.

In Fig. 1 the thickness of the lines representing equipotentials is a measure of the local flatness of the potential. A remarkable property of this model is the presence of open equipotential lines which coexist with closed ones. This property does not mean that "runaway" particles are to be expected among the others (for guiding centers the velocity $\dot{x}$ is perpendicular to the local field $\mathbf{E}$) as would be the case if the potential was time independent.

From the potential (5) we get the electric field

$$\mathbf{E}(x,y,t) = -\frac{a_I}{L} \sum_{\substack{n=1 \\ n^2+m^2 \leq N^2}}^{N} \sum_{m=1}^{N} \frac{1}{(n^2+m^2)^{3/2}} \begin{bmatrix} n \\ m \end{bmatrix} \left\{ \cos\left[\frac{2\pi}{L}(nx+my)+\varphi_{nm}\right]\cos\omega_0 t \right.$$

$$\left. + \sin\left[\frac{2\pi}{L}(nx+my)+\varphi_{nm}\right]\sin\omega_0 t \right\}$$

$$\equiv \mathbf{E}_1(x,y)\cos\omega_0 t + \mathbf{E}_2(x,y)\sin\omega_0 t \ , \tag{8}$$

so that the knowledge of four scalar functions (the components of $\mathbf{E}_1$ and $\mathbf{E}_2$) is sufficient to determine the electric field at all times, hence the motion of the particles.

We define an average energy density $\mathscr{E}$ as

$$\mathscr{E} = \frac{1}{8\pi}\langle |\mathbf{E}|^2 \rangle = \frac{1}{L^2}\int_0^L dx \int_0^L dy \frac{1}{8\pi} E^2(x,y,t) \ , \tag{9}$$

which gives, with Eq. (8),

$$\mathscr{E} = \frac{a_I^2}{8\pi L^2}\sigma_I^2 \ , \tag{10}$$

where

$$\sigma_I^2 \equiv \frac{1}{2} \sum_{\substack{n,m=1 \\ n^2+m^2 \leq N^2}}^{N} (n^2+m^2)^{-2} \ .$$

The r.m.s. electric field $\tilde{E}$ is thus given by

$$\tilde{E} = (8\pi\mathscr{E})^{1/2} = \frac{a_I\sigma_I}{L} \ . \tag{11}$$

As is usual in the numerical studies of modeled systems, it makes life much easier if one uses a particular units system made of the numbers characterizing the model. Thus, we take here L as unit of length, T_0 (the period of waves) as unit of time, and $\tilde{E}$ as unit of electric (and magnetic) field [thus writing $\mathbf{E}(x,y,t)=\tilde{E}\mathbf{e}(x,y,t)$]. If, in addition, we introduce a unit vector perpendicular to the plane of the system, i.e., $\hat{\mathbf{b}}=\mathbf{B}/|\mathbf{B}|$, we arrive at

$$\frac{d\mathbf{x}}{dt} = \left[\frac{2\pi}{L\omega_0}\frac{c\tilde{E}}{|\mathbf{B}|}\right]\mathbf{e}(x,y,t)\times\hat{\mathbf{b}}=\mathcal{A}\mathbf{e}(x,y,t)\times\hat{\mathbf{b}} \ , \tag{12}$$

where t, $\mathbf{x}$, $\mathbf{e}$, and $\hat{\mathbf{b}}$ are now dimensionless. The parameter $\mathcal{A}$ is the ratio of the turbulent drift velocity $v_d=c\tilde{E}/B=2\pi/T_d k_{\min}$ to the maximal phase velocity $v_R=\omega_0 L/2\pi=L/T_0$.

While the parameter $\mathcal{A}$ is convenient for the numerical studies, it has the disadvantage of being defined in terms

of the length L of the box. As will be shown in detail in Sec. VI, a different parameter A should be used in the theoretical analysis:

$$A \equiv \frac{2\pi}{\omega_0\lambda_{\max}}\frac{c\tilde{E}}{B} \ . \tag{13a}$$

This parameter can also be viewed as the ratio of the two time scales T_0 and T_d:

$$A = T_0/T_d \ . \tag{13b}$$

We note that the relation between A and $\mathcal{A}$ involves the ratio $L/\lambda_{\max}$, i.e., the number N_0 of Eq. (6),

$$A = N_0\mathcal{A} \ . \tag{14}$$

III. NUMERICAL INTEGRATION AND PARTICLE TRAJECTORIES

In principle, for each particle considered and at each time step in the numerical integration of Eq. (12) one should compute the electric field according to Eq. (8), which would be impossible with the values of N, of the number of initial conditions, and of the average integration time that we had to consider. Therefore we have adopted the following technique: a set of random phases (φ_{nm}) is generated and $\mathbf{E}_1,\mathbf{E}_2$ are computed on a square grid of $M \times M$ points

$$(0,\Delta x,2\Delta x,\ldots,L)\times(0,\Delta y,2\Delta y,\ldots,L)\in(0,L)\times(0,L) \ ,$$

with a grid spacing $\Delta x = \Delta y = L/M \ll \lambda_{\min}$, i.e., smaller than the minimum wavelength in the expansion (5). In this way the four scalar functions $E_{1,2}^x, E_{1,2}^y$ are replaced by four $M \times M$ matrices which are computed only once and stored in the computer memory. These matrices allow us to compute $\mathbf{E}(x,y,t)$, at any (x,y,t), by means of a linear interpolation between the four nearest-neighboring sites in the matrices, around the point (x,y).

This interpolation procedure might produce numerical

precision problems if Δx was not sufficiently smaller than λ_{min}; by comparing the results obtained with different values of Δx and higher-order interpolation schemes we have empirically determined how small it had to be. In this way we arrived at the following choice: $\Delta x = \lambda_{min}/10 = 0.004$, i.e., we have taken $M = 250$ and $N = 25$; with a $(250)^2$-points grid we have a good resolution even for the smallest wavelength. The various tests we just described have shown that, in the general frame of this work, improving the precision of the techniques we used did not lead to any significant difference of the results.

The integration algorithm adopted is a second-order Euler-Cauchy predictor corrector. The time integration step was $\Delta t = 0.005$ for $A < 1$ and $\Delta t = 0.005/A$ for $A > 1$. This choice is motivated by the fact that for $A \ll 1$ the smallest time scale in the system is T_0 (equal to 1); for $A \gg 1$, we want to maintain $\Delta t \sim O(10^{-2})$ times the smallest time scale in the system which is now $T_d < T_0$.

We made several tests to check the reproducibility of our results which turned out to be nearly insensitive to changing the grid spacing $1/M$, to using or not the restriction $n^2 + m^2 \leq N^2$, to reducing further the time integration step by a factor of 10 with respect to the above-mentioned criteria (i.e., $\Delta t = 0.0005$ for $A < 1$ and $\Delta t = 0.0005/A$ for $A > 1$), and to varying the number of trajectories in the range 100–2000, the usually adopted value being 400 initial conditions. The simulations have been performed using mostly Cray X-MP computers. A CYBER 170 and a VAX 11/750 have also been used.

Something of the potential field structure is retained in particle trajectories. Actually a rapidly oscillating motion (of period T_0) is found together with a slower drift, due to the turbulent electric field fluctuations. The effect of the anisotropy of the potential is recognized by the fact that the elongation of the fast oscillatory motion is directed around the $y = -x$ direction. How strongly particle trajectories are affected by the nonlinear nature of the equation of motion, thus deviating from being merely single equipotential lines, is then realized by looking at Fig. 2(a).

We report some stroboscopic sections, i.e., "trajectories" in the (x, y) (phase) space made up of dots placed at the single-particle positions recorded at each period $(t = T_0, 2T_0, 3T_0, \ldots)$. We also report some stroboscopic sections obtained by folding the trajectories in the periodicity cell of potential.

In Fig. 2(a) we see trajectories that are periodic on a length scale comparable with the periodic cell L, and there is no evident relationship with the structure of the electric potential; in particular, nothing seems to remain of its anisotropy. Of course, periodic trajectories can be found with a smaller length. These results correspond to $A = 0.2$; this amplitude belongs to the range of values for which we have found a vanishing asymptotic diffusion coefficient, just because the trajectories are confined. For this amplitude we have also found a small but definitely positive value of the Kolmogorov entropy h; in other words for $A = 0.2$ we have chaotic dynamics and local exponential separation of nearby trajectories (see Sec. IV).
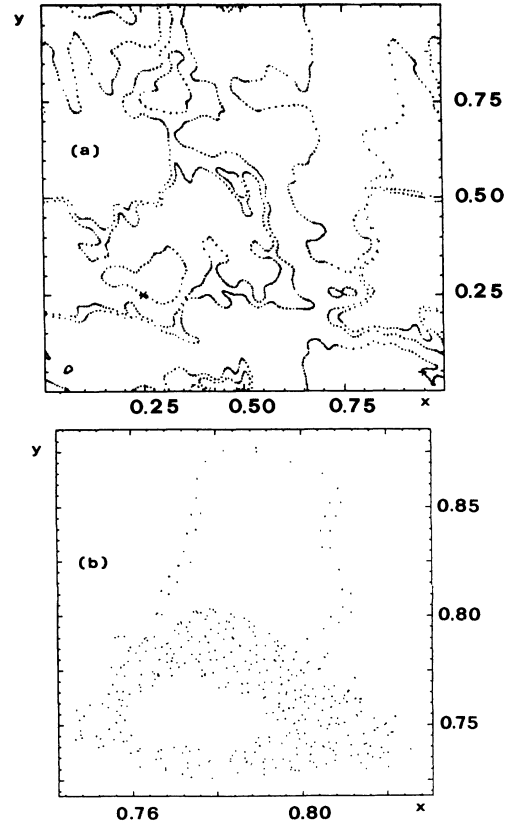
FIG. 2. (a) Stroboscopic sections of sample trajectories obtained with $A = 0.2$. The trajectories have been folded into the unit square. 1000 points are displayed for 10 randomly chosen initial conditions. (b) Small stochastic region for $A = 0.2$ and $x_0 = 0.75$, $y_0 = 0.75$.

This notwithstanding, on a large scale all the observed trajectories are bounded and closed (i.e., quasiperiodic on the observational time scale), so that we can think of a coexistence in phase space of regular and chaotic regions, with a measure of the latter ones vanishing with A. This idea is a rather common one for nonlinear Hamiltonian systems and it is confirmed in our case by what is shown in Fig. 2(b). Here a stroboscopic section is reported for a trajectory obtained at $A = 0.2$ (same value as before) but for a different initial condition $(x_0 = 0.75, y_0 = 0.75)$ and composed of 500 points. It covers a small fraction of the (x, y) plane and displays the random scattering of points, characteristic of chaotic motion, with two big holes which are likely to be the analogue of invariant tori in autonomous systems. Chaotic regions thus exist even at $A = 0.2$ where nearly all trajectories are closed and the asymptotic diffusion coefficient is vanishing.

In the considered range of values of the amplitude A, there does not seem to be a sharp stochasticity threshold, while different chaotic regimes can take place. These regimes are detected by the change in the functional dependence of the Kolmogorov entropy h and of the diffusion coefficient D in the interval $A = 0.2$–0.3: $D(A = 0.2) = 0$ and $D(A = 0.3) > 0$. Around this threshold a transition occurs between dynamical trapping of the trajectories and unbounded diffusive motion, giving rise to large-scale

stochasticity.

The lack of a threshold for stochasticity (i.e., for positive Kolmogorov entropy), and the "smooth" increase of the measure of the chaotic regions in phase space is qualitatively shown in Fig. 3 where four different stroboscopic sections are shown for the same initial condition, but for slightly increasing values of A. The starting point is $(x_0=0.25, y_0=0.25)$; in Fig. 2(a) this produced a close trajectory which resembles that of Fig. 3(a) for $A=0.25$. In Fig. 3(b) $A=0.3$ and the number of points is 1000, but the trajectory is no longer regular: the points scatter around several "pseudo-invariant" boundaries; the shape of the previous trajectory is still recognizable.

In Fig. 3(c), with $A=0.32$, we see that the stochastic layer penetrates the original "pseudoinvariant" boundary and two new ones show up inside. For $A=0.34$, Fig. 3(d), the thickness of the stochastic layer is increased, compared to those of Figs. 3(b) and 3(c), and after the same lapse of time (1000 periods) the trajectory has spread over a wider region of the (x,y) plane.

In Fig. 4 the initial condition has been changed and the value of A further increased. A similar scenario is found. Starting with a closed, regular, and almost elliptic orbit,

obtained at $A=0.4$ [Fig. 4(a)], we see that going to $A=0.41$ [Fig. 4(b)], this regular orbit breaks into many small and very elongated "islands;" this is analogous to the breaking of invariant curves in other conservative and autonomous systems. In Fig. 4(c), $A=0.42$, a section typical of the appearance of a homoclinic tangle is found; in Fig. 4(d), again at $A=0.42$ but for a longer integration time, we can see a very nice section: the trajectory displaces itself in a rather erratic way, but three traps show up. The traps are easily identified as those regions where there is a high density of points and consequently where the trajectories spend a long time without diffusing.

This Fig. 4(d) is a good example of intermittency of our dynamical system. A particle spends a long time near a local trap, then quickly moves to another region where it is again trapped, and so on. This phenomenon is a very clear mark of non-Gaussian dynamics, and this intermittency acts to slow down absolute diffusion of the guiding centers (see Sec. IV D).

As A is increased, the stochastic layer gets thicker and thicker until the phase space is completely ergodic. This is pictorially well shown by the stroboscopic sections reported in Figs. 2–5.
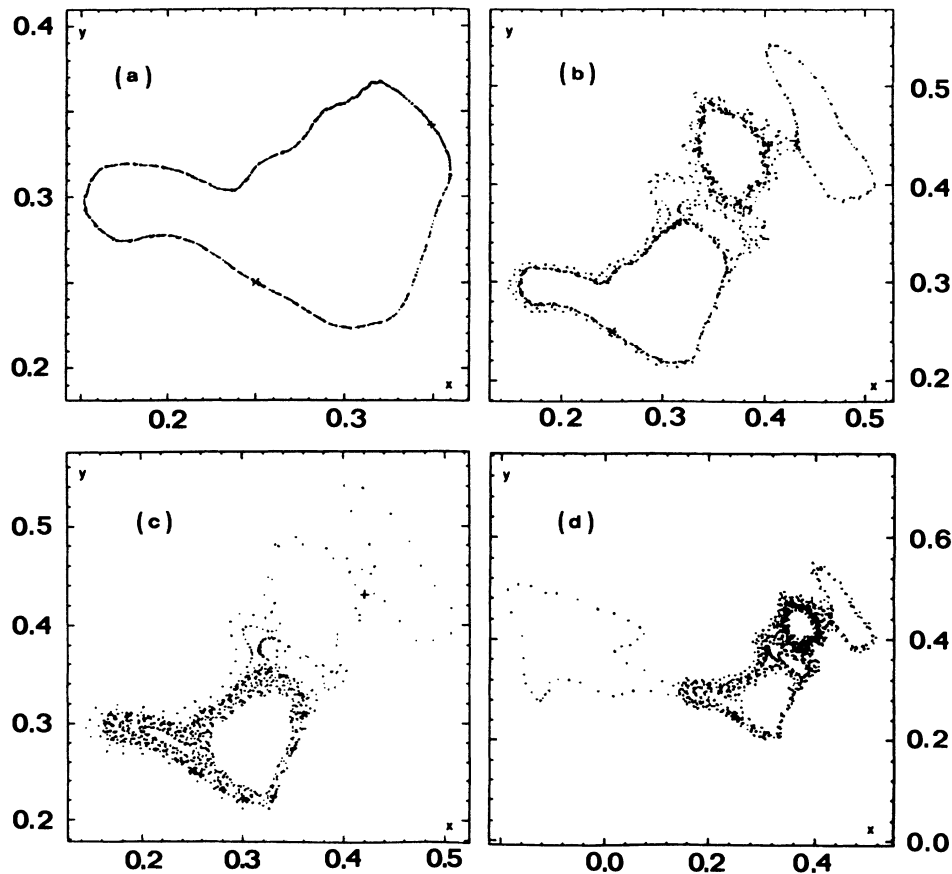
FIG. 3. An ordered trajectory losing its stability as A is increased. The orbit of (a) can also be seen (marked with an asterisk) in Fig. 2(a), but is shown here for $A=0.25$; (b) $A=0.3$, a stochastic diffusion starts up and new "holes" show up; (c) $A=0.32$, the previous stochastic layer get thicker; (d) $A=0.34$, a larger scale orbit is obtained. All these figures contain 1000 points. The initial condition is everywhere the same.

IV. STATISTICAL PROPERTIES OF PARTICLE MOTION

A. Absolute diffusion

In order to study the absolute diffusion properties of the system, we have considered a set of $\mathcal{N}$ particles uniformly distributed at random in the domain $0 \leq x, y \leq 1$, at $t = 0$. We have measured the time dependence of absolute diffusion by computing

$$\langle r^2(t) \rangle = \frac{1}{\mathcal{N}} \sum_{i=1}^{\mathcal{N}} |\mathbf{x}_i(t) - \mathbf{x}_i(0)|^2 , \tag{15}$$

where $\mathbf{x}_i(t)$ $(i = 1, \ldots, \mathcal{N})$ is the position of the ith particle at time t as obtained by integrating Eq. (12) with the initial condition $\mathbf{x}_i(0)$.

In general, the long-time dependence of $\langle r^2(t) \rangle$ is linear as shown in Fig. 6, and the dimensionless diffusion coefficient is defined by its asymptotic slope

$$\mathcal{D} = \lim_{t \to \infty} \frac{1}{t} \langle r^2(t) \rangle . \tag{16}$$

We have evaluated $\mathcal{D}$ for several values of $\mathcal{A}$ ranging from $\mathcal{A} = 0.1$ to $\mathcal{A} = 10$, mostly with $\mathcal{N} = 400$ and for integration times ranging from $t = 500$ to 3000.

The results are reported in Fig. 7 where the following dependences on $\mathcal{A}$ appear to apply:

$$\mathcal{D}(\mathcal{A}) \propto \begin{cases} \mathcal{A}^2, & \mathcal{A} \leq 1 \\ \mathcal{A}, & \mathcal{A} \geq 1 . \end{cases} \tag{17}$$

These dependences, valid for a broad spectrum, are known as the quasilinear scaling (small values of $\mathcal{A}$, or weak turbulence regime) and the Bohm scaling (large values of $\mathcal{A}$, or strong turbulence regime). This result is very different from what has been found with a two-wave model,[14] which suggests that it is possible to represent systems by simple dynamical models (though a little more involved than that of Ref. 14) and obtain a description in reasonable agreement with the existing theories. We have just said that for $0.2 < \mathcal{A} < 0.3$ we observe that particles remain confined in space on almost periodic trajectories with very long periods (typically several hundred times T_0). As a consequence, $\langle r^2(t) \rangle$ grows in time up to a saturation level (whose value depends on $\mathcal{A}$). This saturation phenomenon has been followed up to $t \sim 6 \times 10^4 T_0$ with $\mathcal{N} = 120$. Thus there is a critical value of $\mathcal{A}$ in the interval (0.2, 0.3) below which diffusion stops ($\mathcal{D} = 0$).

We also measured the quantity
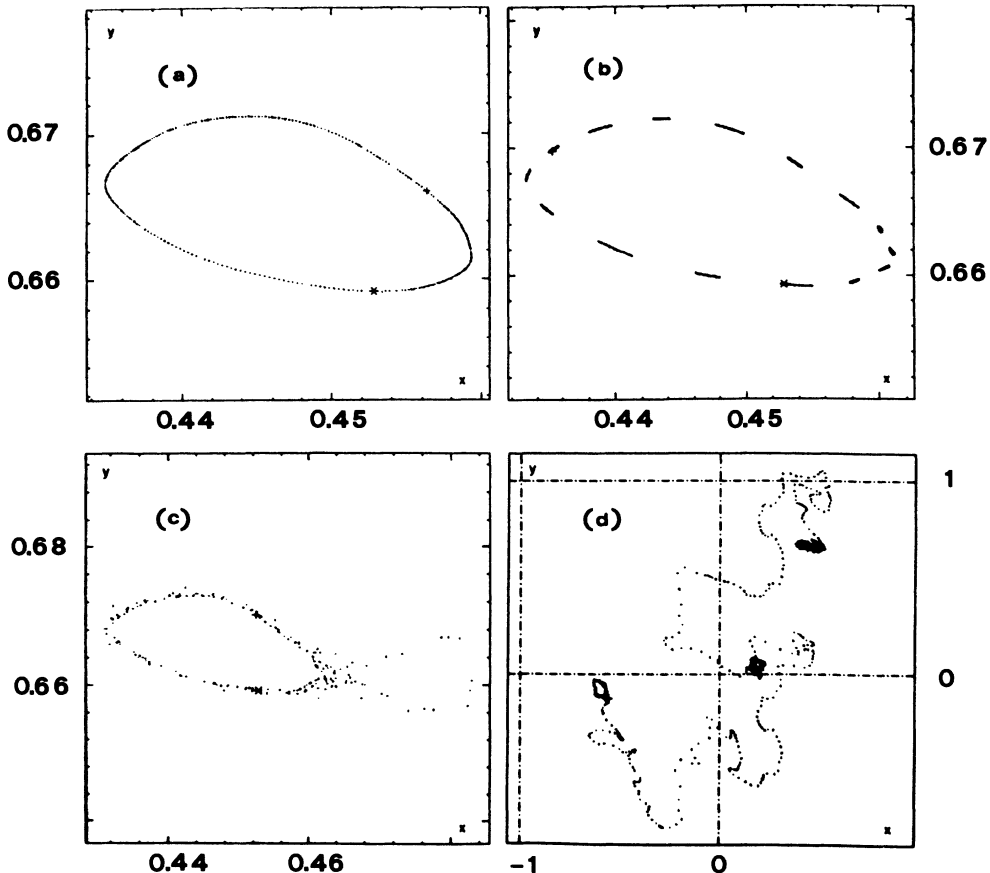
FIG. 4. Stroboscopic sections of another regular orbit destabilized by increasing A. (a) $A = 0.4$, a regular orbit is found; (b) $A = 0.41$; (c) $A = 0.42$, the previous regular orbit has undergone a stochastic transition; (d) $A = 0.42$ again, but the trajectory has been followed for a longer time. Three traps (denser regions) show up.
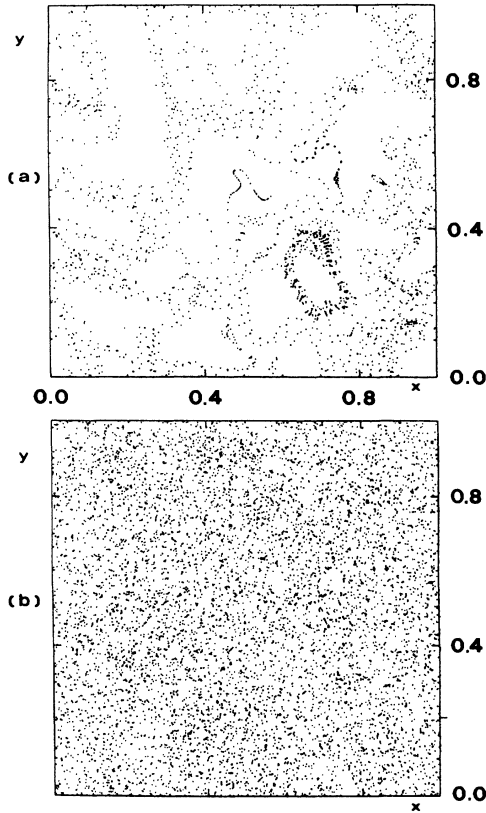
FIG. 5. Stroboscopic sections for (a) $A = 0.45$ (QL region), $x_0 = 0.741$, $y_0 = 0.749$ (3000 points); (b) $A = 5.0$ (Bohm region), $x_0 = 0.741$, $y_0 = 0.749$ (9000 points).
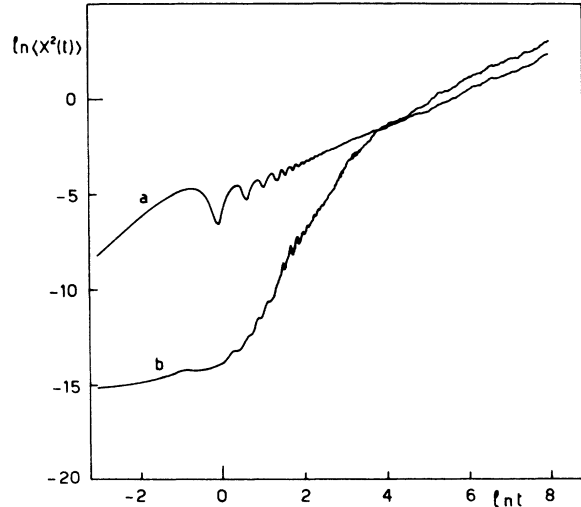
FIG. 6. Simulation results for absolute a [$x^2 \equiv r^2$ of Eq. (15)] and relative b [$x^2 \equiv \delta r^2$ of Eq. (18)] diffusion for model I at $A = 0.45$.

$$\frac{1}{\mathcal{N}} \sum_{i=1}^{\mathcal{N}} [\xi_i(t) - \xi_i(0)] \bigg/ \left[\frac{1}{\mathcal{N}} \sum_{i=1}^{\mathcal{N}} [\xi_i(t) - \xi_i(0)]^2 \right]^{1/2}$$

for both $\xi_i = x_i$ and $\xi_i = y_i$. We always found an erratically oscillating value around zero with a mean deviation of about 10^{-2}. In other words, there was no average displacement.

Test runs have been performed with $\omega_0 = 0$, where we went from three coordinates (x, y, t) to two coordinates
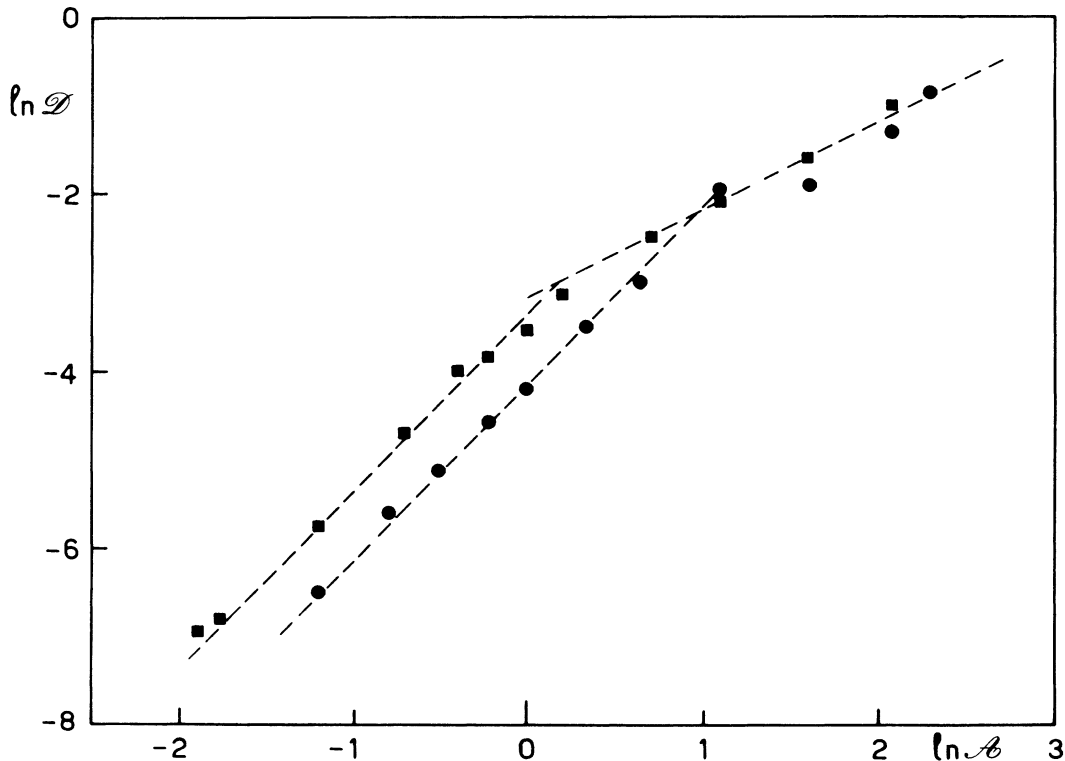
FIG. 7. Absolute diffusion coefficient $\mathcal{D}$ vs turbulence amplitude parameter $\mathcal{A}$. Circles refer to model I and squares to model II (Sec. V).

(x,y) in our dynamical system; this implies that chaotic solutions are forbidden because of the uniqueness of solutions of differential equations; thus diffusion must stop. If the equations of motion (12) are integrated with $\omega_0=0$ we find a residual diffusion whose level is lowered by increasing M. In other words, the representation of the field by discrete matrices and the interpolation algorithm act as if a noise were added to the system. An overestimate of the diffusion coefficient is the main consequence, but this amounts to less than 1% with the adopted parameters.

B. Relative diffusion

The relative diffusion properties are obtained from the time dependence of the r.m.s. relative distance $\delta r(t)=x_i^{(1)}(t)-x_i^{(2)}(t)$, and

$$\langle \delta r^2(t) \rangle = \frac{1}{\mathcal{N}} \sum_{i=1}^{\mathcal{N}} | x_i^{(1)}(t)-x_i^{(2)}(t) |^2 , \tag{18}$$

where $x_i^{(1)}(t)$ and $x_i^{(2)}(t)$ are the positions of the two particles in the ith pair at time t. We are mainly interested in the relative diffusion of neighboring particles; the initial separations $\delta r_i(0)=x_i^{(1)}(0)-x_i^{(2)}(0)$ were taken as much smaller than the smallest wavelength

$$| \delta r_i(0) | /\lambda_{min}=N | \delta r_i(0) | /L \ll 1 .$$

Typically we have used $| \delta r_i(0) | /L =0.0005 \ll 1/N =0.04$. In Fig. 8 we exhibit a typical time behavior of $\ln\langle \delta r^2(t) \rangle$.

The clump effect predicted theoretically[16] for relative diffusion appears quite clearly on this curve (see Sec. VII for the application of the theory to the present model). This effect is verified to take place independently of the value of A, and some sort of "universal" behavior is found in the range of A values that we have considered (see Fig. 8),

$$\ln\langle \delta r^2(t) \rangle =F(t/\tau_{dif}) , \tag{19}$$

where $\tau_{dif}\sim\mathcal{D}^{-1}$ is the diffusion time scale. We thus find that in both the quasilinear and the Bohm diffusion regimes, the relative diffusion satisfies a simple scaling law which modifies its time dependence according to the absolute diffusion coefficient.

C. Kolmogorov-Sinai entropy

We have verified that particles moving according to Eq. (12) undergo a stochastic dynamics. Deterministic chaos is rather ubiquitous in nonlinear dynamical systems (with the obvious exception of integrable systems). Roughly speaking, this means that an extreme sensitivity to initial conditions is present and that nearby trajectories exponentially diverge in time. These properties are formalized by defining the following quantity (maximal Lyapunov characteristic exponent):[19]

$$h = \lim_{t\to\infty} h(t)= \lim_{t\to\infty} \frac{1}{t}\ln\frac{\|\zeta(t)\|}{\|\zeta(0)\|} , \tag{20}$$

where $\zeta(t)$ is a vector in a tangent space whose evolution is given by
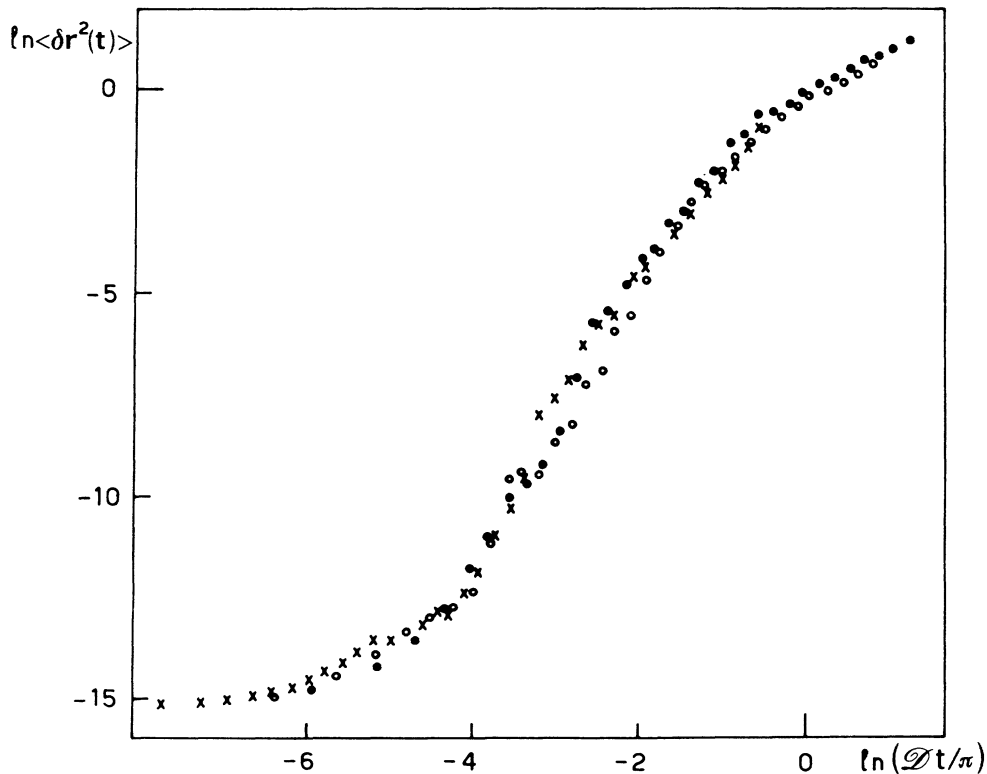
FIG. 8. Scaling law for the clump effect in relative diffusion. Crosses refer to $A=0.6$ (QL regime), open circles refer to $A=1$ (transition regime), and solid circles correspond to $A=5$ (Bohm regime).

$$\dot{\xi}_i = \sum_{j=1}^{2} \left[\frac{\partial \dot{x}_i}{\partial x_j} \right]_{\mathbf{x} = \mathbf{x}(t)} \zeta_j \qquad (21)$$

and $(\partial \dot{x}_i / \partial x_j)$ are computed along a trajectory given by the equation of motion. A positive value of h is a mark of the instability which makes the motion stochastic; $h = 0$ means that the motion is regular. A practical estimate of the Kolmogorov-Sinai entropy is obtained by means of a standard technique;[20] this consists in averaging along a trajectory the quantity $\ln d_n$, with $d_n = \|\mathbf{W}_{n\tau}\| / \|\mathbf{W}_{(n-1)\tau}\|$; $\mathbf{W}_n$ is the distance vector between the reference trajectory and some nearby trajectory, and $\mathbf{W}$ is renormalized to a given initial norm after each time interval τ. As the stochastic component (i.e., a compact phase-space area of the unstable motion) can have a very intricate structure, h could depend on the trajectory, i.e., on the initial conditions, even with very long integration times;[21] consequently, we have performed an averaging of h over 10 initial conditions. By means of $\langle h \rangle$ we obtain global information about the degree of chaoticity of the system; $\langle h \rangle$ is an estimate of the Kolmogorov-Sinai entropy.

In Fig. 9 we plot the long-time mean value $\langle h \rangle$ versus A. We observe again a change of regime around the value $A \sim 1$. Actually, for small values of A we find $\langle h \rangle \sim A^2$ $(A \ll 1)$ while for $A > 1$ a slower functional dependence is found, consistent[22] with the logarithmic dependence of Ref. 14. The errors made in determining $\langle h \rangle$ are of the order of 5%. These are not computational errors but represent the dispersion of the values h_i (obtained with different initial conditions). This dispersion is

larger when A is lowered to very small values. It is worth mentioning that the relation $\langle h \rangle \sim A^2$ is in agreement with a prediction of the previously mentioned theory[16] in the "small clump regime" (see Sec. VII). We did not find any sharp threshold on the value of A for the existence of a positive average Kolmogorov entropy: a chaotic component in phase space seems always to be present in the range of amplitudes that we considered.

The fluctuations of the values of h_i are negligible for $A > 1$. The strong fluctuations observed for small A, and in particular when $D = 0$, could be related with the existence of small chaotic regions among regular trajectories; these regions look disjointed and bounded by closed quasiperiodic trajectories. Finally, we note that the dependence of $\langle h \rangle$ on A also denotes the existence of a smooth transition between quasilinear and Bohm diffusion regimes. In the limit of large A (low frequency ω_0) the diffusion mechanism could be analogous to the one studied in detail for a simpler dynamical system in Ref. 23.

D. Non-Gaussian properties of dynamics

As Gaussian approximations are rather commonly introduced in the theories of turbulent diffusion in plasmas, it is sensible to investigate some statistical properties of particle motion related to the degree of Gaussian behavior of the stochastic dynamics. One of the simplest ways of testing to what extent a random variable $\xi(t)$ (with zero mean value) is a Gaussian process consists of evaluating the magnitude of the fourth ·cumulant, i.e.,
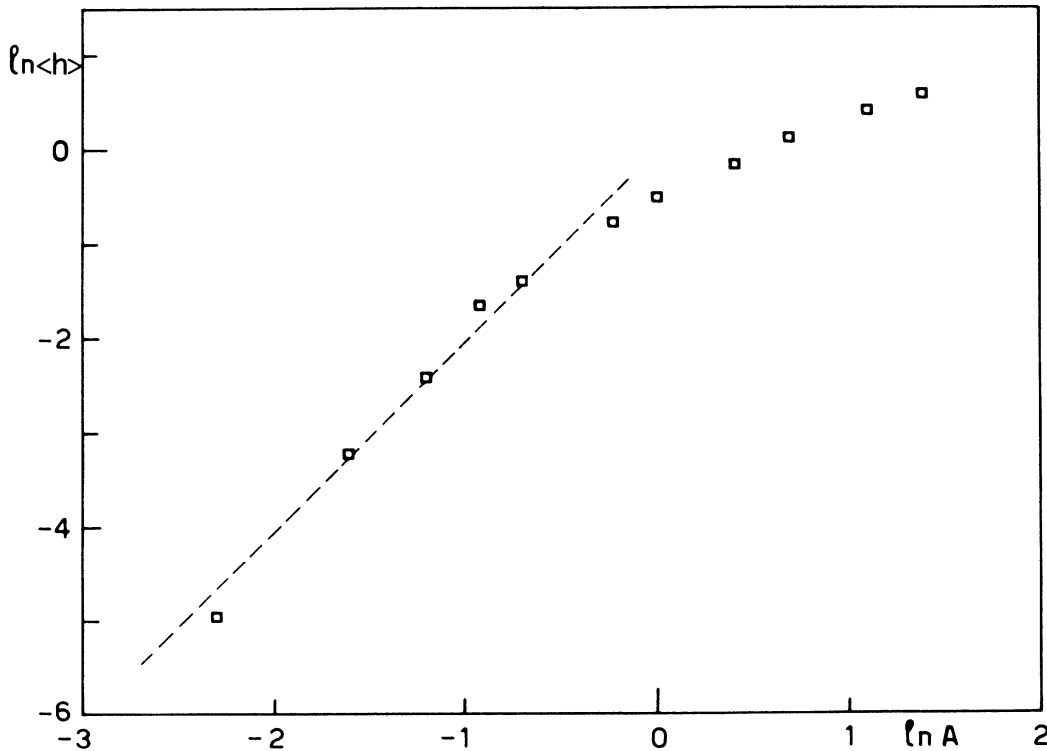
FIG. 9. Plot of Kolmogorov-Sinai entropy vs A. The slope of the reference line is 2.

$C_\xi = \langle \xi^4 \rangle - 3\langle \xi^2 \rangle^2$ (in one dimension), which vanishes (with all higher-order cumulants) for a Gaussian process. The deviation from the Gaussianity can thus be measured by evaluating the kurtosis, i.e., $K_\xi = \langle \xi^4 \rangle / \langle \xi^2 \rangle^2$, which reduces to 3 for a Gaussian process. When K is larger (smaller) than 3, it means that the wings of the probability distribution of ξ are more (less) important as compared to the Gaussian distribution; kurtosis is "broadness."

We have measured the kurtosis of the following quantities: (a) the scalar velocity $v = |\dot{x}|$; (b) $\delta x, \delta y$, the relative displacements in directions x and y (as functions of time); (c) $\Delta x, \Delta y$, the absolute displacements in directions x and y (as functions of time). For the time-averaged kurtosis K_v of the scalar velocity, we obtain values which are systematically below 3.

These are weakly varying with A as follows: for $A = 0.5, 1, 2, 3$ we have, respectively, $K_v = 2.322, 2.365, 2.379, 2.380$. Thus we have a significant deviation of the fourth cumulant from its Gaussian value. A typical behavior of the kurtosis of absolute displacement $K_{\Delta x}, K_{\Delta y}$ is shown in Fig. 10. The curves mainly remain below the Gaussian value. For short times (less than one period) the kurtosis is about 2.3; this value is close to the previously reported ones for K_v, probably for the simple reason that the absolute displacement is nothing else than the time integral of the velocity. On the other hand, we have peak at $t = T_0$ and at longer times the Gaussian value is reached.

As for the kurtosis of the relative displacement, in Fig. 11 a typical behavior of $K_{\delta x}$ and $K_{\delta y}$ is shown; around

the clump lifetime, i.e., in the fastest growth of the relative diffusion, a very strong deviation from Gaussian statistics is observed. This phenomenon takes place independently of the value of the turbulent amplitude A. It reminds us of the fluctuations enhancement which is typical around an instability point. The analogy between the exponential separation in the clump regime and a usual instability has already been suggested.[24] This phenomenon also reminds us of the anomalous fluctuations[25] which are produced during the decay of a metastable state. The separation of two neighboring particles at $t = 0$ can be thought of as the decay of the dynamically unstable state of two nearby initial conditions in a chaotic dynamical system.

The strong peaks of $K_{\delta x}, K_{\delta y}$ indicate that the fluctuations are dramatically amplified with respect to those expected for a Gaussian process. For longer times both $K_{\delta x}$ and $K_{\delta y}$ attain the Gaussian value of 3.

These different facts, i.e., that K_v is below 3 and time independent while $K_{\Delta x, \Delta y}$ and $K_{\delta x}, K_{\delta y}$ keep non-Gaussian values only during finite times, are due to the fact that $v(t) = |\dot{x}|$ is a stationary process while $\Delta x, \Delta y, \delta x, \delta y$, are not. The transient deviations for the latter quantities are somehow reflecting the existence of a finite decorrelation time scale for the trajectories. In fact, this time scale is approximately the inverse of the Kolmogorov-Sinai (KS) entropy, and the clump time scale (at which the peaks of $K_{\delta x, \delta y}$ occur) can be related to the KS entropy.

Another signature of non-Gaussian stochastic dynam-
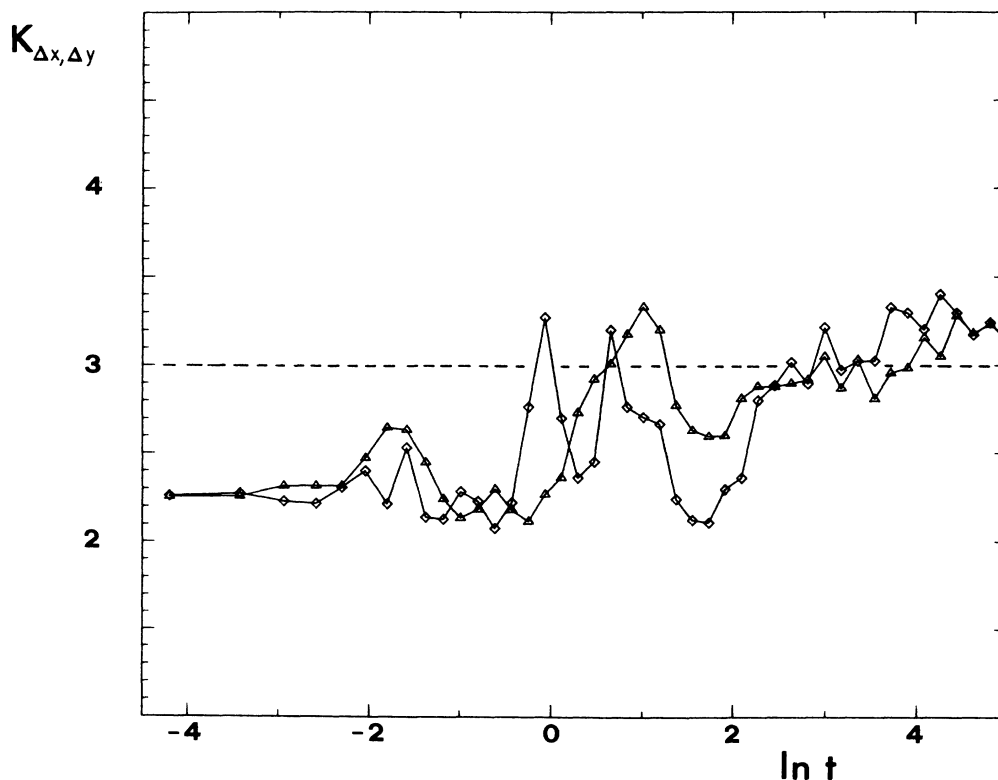
FIG. 10. Absolute diffusion kurtosis vs logarithm of time. $\Diamond$, $K_{\Delta x}$; $\triangle$, $K_{\Delta y}$; $- - -$, Gaussian level. Here $A = 1$ and 800 particles were involved.

CHAOTIC DIFFUSION ACROSS A MAGNETIC FIELD IN A . . .

ics has been found by computing the velocity autocorrelation function $C(\tau) = \langle \langle \dot{\mathbf{x}}(t) \cdot \dot{\mathbf{x}}(t+\tau) \rangle_t \rangle_p$, where the double averaging stands for averaging over particles ($\langle \cdots \rangle_p$) and over time ($\langle \cdots \rangle_t$). Taking advantage of the stationarity of $\dot{\mathbf{x}}(t)$ we have computed

$$C(\tau) = C(n\delta t) = C_0 \sum_{j=1}^{\mathcal{N}} \sum_{i=1}^{\mathcal{M}} \dot{\mathbf{x}}_j(t_i) \dot{\mathbf{x}}_j(t_i + n\delta t) , \quad (22)$$

where C_0 is a normalization factor, δt is the elementary time lag, $\mathcal{M}\delta t$ is the time interval over which $C(\tau)$ is

evaluated, and $\mathcal{N}$ is the number of different particles (i.e., of initial conditions). With the parameters we used, each point of the autocorrelation function resulted from the averaging over 40 000–60 000 terms in the sum (22). In Fig. 12 the velocity autocorrelation (22) is plotted versus time lag and compared with an exponentially decaying envelope.

Actually, if the dynamics were Gaussian the velocity autocorrelation functions would be expected to be exponentially decaying. On the contrary, the temporal decay of the autocorrelations is slower in the numerical
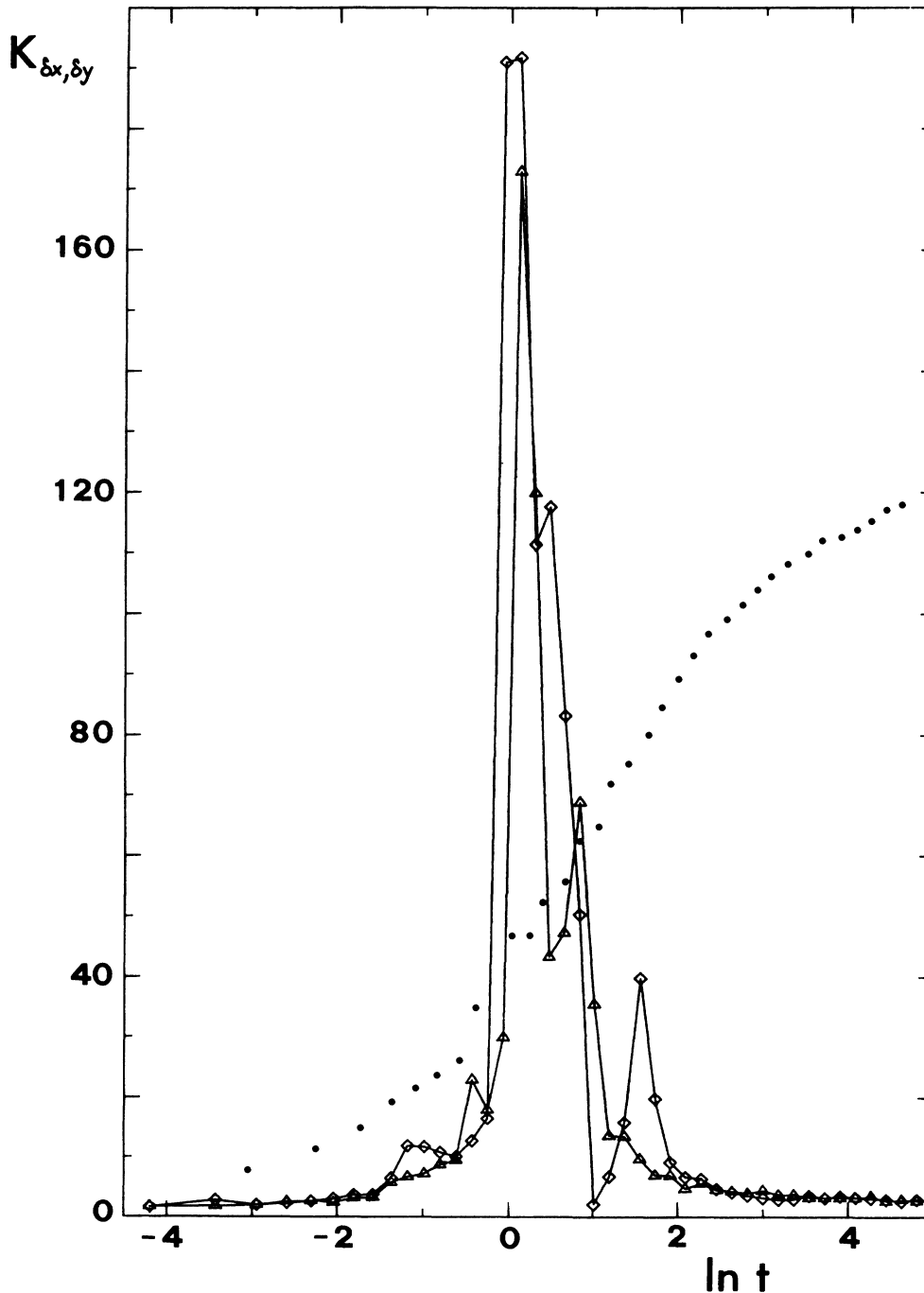
FIG. 11. Relative diffusion kurtosis vs logarithm of time. $\lozenge$, diffusion in x direction; $\triangle$, diffusion in y direction. Here $A = 1$ and 400 pairs of particles were involved. $\cdot \cdot \cdot \cdot$ on the background is the corresponding relative diffusion.

simulation where long nonexponential time tails show up. The fact that the autocorrelation functions in the stochastic components of dynamical systems are in general more complicated than simple exponentials is common in low-dimensionality chaos,[26] and also in real turbulent fluids.[27]

As the diffusion coefficient $\mathcal{D}$ is the time integral of the velocity autocorrelation function (see Sec. VI), a deviation of the numerical result for $\mathcal{D}$ from the theoretical prediction (obtained with a Gaussian approximation) is expected. We recall that a pictorial aspect of non-Gaussianity is given by Fig. 4(d) where an intermittent trajectory is shown. It is quite remarkable, however, that the correct diffusion law appears not to be affected [i.e., $\langle r^2(t) \rangle = \mathcal{D}t$, large t]. This fact is not *a priori* obvious; it is well known[28] that intermittency is often responsible for the appearance of nonclassical diffusion laws [i.e., where $\langle r^2(t) \rangle$ is a nonlinear function of t]. Such nonclassical diffusion is produced by a hierarchy of trapping times distributed over a wide range of time scales.[29] Therefore we can guess that in our model essentially one trapping time scale is dominant instead of a wide-spread distribution of trapping times.

V. A MODEL WITH ISOTROPIC POTENTIAL

In this section we briefly describe the results we have obtained for another model, with the same spectral slope but with a different choice for the summation domain in **k** space. We wanted to verify to what extent our results for the previous model (which we shall call model I) were

"structurally stable," in other words, whether changing some of the initial assumptions would leave the phenomenology essentially unchanged.

We wanted to choose this domain in such a way that the electric potential would be instantaneously isotropic. Both a circle and half a circle in the (n,m) plane would answer this purpose: with the former choice the waves are stationary (and so is the potential), while the latter choice maintains the propagating nature of the components. Since we did not want to change too many things at the same time we chose again propagating waves. Another sensible change consists of not letting the unit length L coincide with the maximum wavelength in the turbulent spectrum; thus we have eliminated some low n and m values according to a constraint $N_0^2 \leq n^2 + m^2 \leq N^2$ in the summation of the Fourier components of Φ. The potential for model II thus became

$$\Phi(x,y,t) = \frac{a_{\text{II}}}{2\pi} \sum_{\substack{n=-N \\ N_0^2 \leq n^2 + m^2 \leq N^2}}^{N} \sum_{m=0}^{N} \frac{1}{(n^2+m^2)^{3/2}}$$

$$\times \cos\left[\frac{2\pi}{L}(nx + my) \right.$$

$$\left. + \varphi_{nm} - \omega_0 t \right] ,$$

(23)

C(τ)
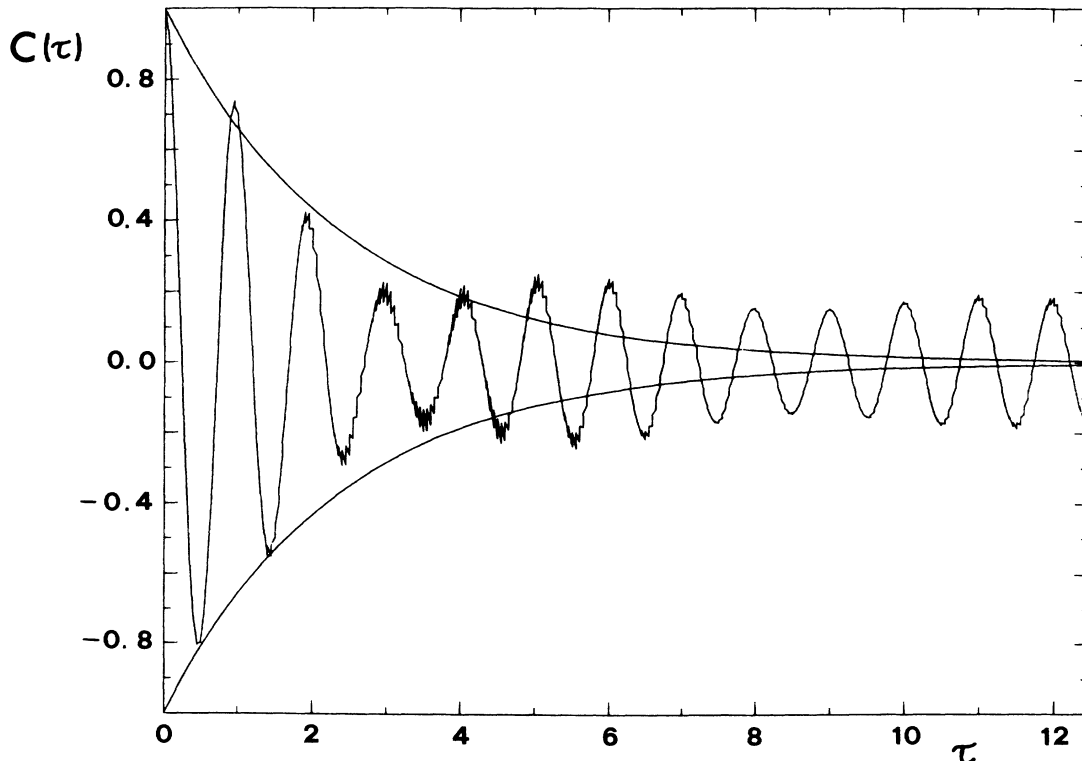
FIG. 12. Velocity autocorrelation function. Here $A = 1$ and the number of particles was 200. An exponential envelope is plotted to display the long-time tail.

where the symbols have the same meaning as in Eq. (5).

In Fig. 13 we show the equipotential curves for this field with a generic realization of the random phases $\{\varphi_{nm}\}$ at $t=0$ and on the unit square $(0,L)\times(0,L)$.

Comparing Figs. 1 and 13, one readily sees why we say that model II is (instantaneously) isotropic: there is no evident preferred direction in Fig. 13; this isotropic character of the electric potential and fields is very easy to establish on mathematical grounds. On the other hand, looking at how equipotential curves change in the course of time, one would see their complicated structure deform while moving (on average) towards the positive y axis. Thus model II is "isotropic" and "propagative."

When we considered choosing the parameters of the potential (N_0,N) and the precision of the numerical integration (essentially the number M^2 of points in the field grid, or the distance Δx between two neighboring points), we were confronted with a very difficult problem. Indeed, to make model II closer to the experimental reality, we should have taken N_0 and N as large as possible (compared to 1), while keeping their ratio $\nu=N_0/N=\lambda_{\min}/\lambda_{\max}$ fixed between $\frac{1}{12}$ and $\frac{1}{25}$. But, choosing modestly $N_0=4$ and $N=25N_0=100$, one readily evaluates that, if we wanted the smallest wavelength to be represented by 10 points, the field matrices would occupy four M words in the central memory of the computer. We thus had to be even more modest and adopt the values $N_0=4$, $N=48$ ($\nu=\frac{1}{12}$), and $\Delta x=\frac{1}{300}$ ($M^2=9\times10^4$); thus $\lambda_{\min}/\Delta x=6.25$. With this choice, the relation between the parameter $\mathcal{A}$ and the energy parameter A [Eq. (13)] becomes $A=4\mathcal{A}$.

From here on, the analysis leading to the equation of motion (11) as well as the numerical computations follow the same lines as for model I, the only modification lying in the domain of $\mathbf{k}$ space one sums over; as a result, the

quantity σ^2 becomes

$$\sigma_{\text{II}}^2=\frac{1}{2}\sum_{\substack{n=-N\\N_0^2\le n^2+m^2\le N^2}}^{N}\sum_{m=0}^{N}\frac{1}{(n^2+m^2)^2}.\qquad(24)$$

In Fig. 14 we present an example of the absolute and relative diffusion curves obtained. The clump effect for relative diffusion is again present; absolute diffusion again starts with a t^2 law for very short times and the regime $\langle r^2(t)\rangle\propto t$ soon follows with strongly damped (at small A) or even no oscillations (larger A, as in Fig. 14). This is the most relevant difference with the corresponding curves obtained for model I: not only do the oscillations of the absolute diffusion curve disappear but the asymptotic linear diffusion regime is reached at much shorter times in model II; hence, the evaluation of the diffusion coefficient is improved.

In Fig. 7 the different values of the diffusion coefficient are reported as a function of $\mathcal{A}$. Two facts are striking: (i) qualitatively, we observe again both limiting regimes, i.e., $D\propto A^2$ for small A (quasilinear regime) and $D\propto A$ for large A (Bohm regime); (ii) quantitatively, the values of the diffusion coefficient in both models are very close. The scaling law for relative diffusion, reported in Eq. (19), has been confirmed also for model II.

We have found again that for sufficiently small A diffusion stops and most of the trajectories are regular; this happens for $\mathcal{A}$ in the range (0.05, 0.15), i.e., the transition to the nondiffusive regime occurs at lower values of $\mathcal{A}$ than in model I.

As for the statistical properties of the dynamics, we have found as in model I a strong enhancement in the relative diffusion kurtosis $(K_{\delta x,\delta y})$ around the clump time scale. Here the maxima attained by $K_{\delta x,\delta y}$ are about 40% of the values obtained for the previous model and have a weak tendency to decrease when A is increased (as before). The results for the absolute diffusion kurtosis $K_{\Delta x,\Delta y}$ are in qualitative agreement with those of model
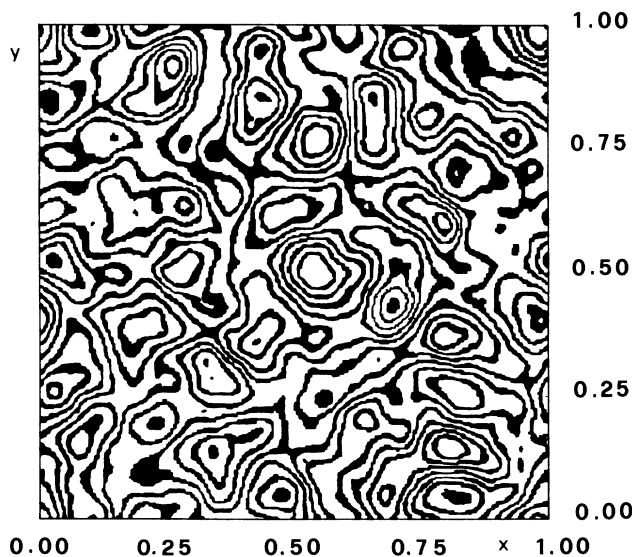
FIG. 13. Equipotential curves for the turbulent field in model II at $t=0$ [from Eq. (23)]. A more isotropic field structure shows up.
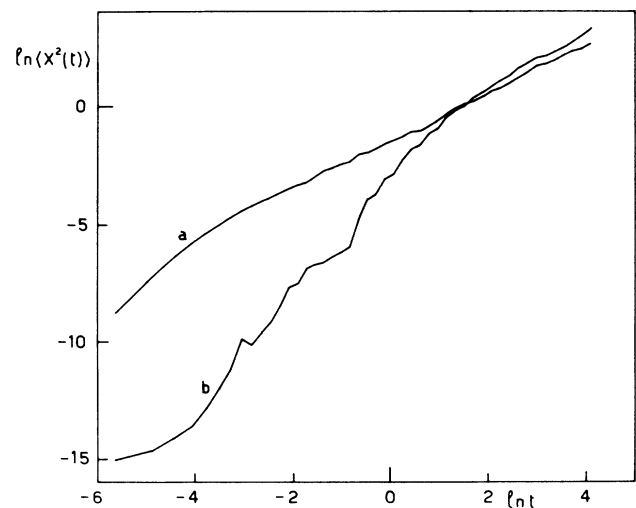
FIG. 14. Simulation results for absolute a [$x^2\equiv r^2$ of Eq. (15)] and relative b [$x^2\equiv\delta r^2$ of Eq. (18)] diffusion for model II at $\mathcal{A}=5.0$.

I, the essential difference being that, in model II $K_{\Delta x, \Delta y}$ reaches the Gaussian value at shorter times, which agrees with the earlier onset of the diffusion regime. The values of K_v are still below 3 and range from about 2.4 to about 2.7; this is in qualitative agreement with the other reductions in the deviations from Gaussianity.

VI. THEORETICAL PREDICTIONS AND COMPARISON WITH THE SIMULATION RESULTS

In this section we apply a recent theory[16] to the models we have proposed and compare the predictions of this theory to the observed properties of both models. We show that (at least) a qualitative agreement exists, both for absolute and relative diffusion. We must, however, insist from the start on the fact that a perfect quantitative agreement should not be expected. Indeed, the theory aims at describing an experimental situation where the dimension L of the system is very much larger than the wavelengths of the dominant turbulent modes (technically, the theory is obtained in the limit $L \to \infty$, with $\lambda_{min}, \lambda_{max}$ finite, the wave-number spectrum thus becoming continuous). In addition, the theory assumes that the turbulence is stationary, homogeneous, and isotropic. On the contrary, in the models we have studied the dimension L is, of course, finite and the electric field spectrum is anisotropic.

A. Absolute diffusion

We here derive the absolute diffusion equation for the isotropic version of our models in the limit of infinite system. Making the models isotropic (at least in the infinite system limit) is, of course, trivial; it suffices to start from Eq. (8) and extend the summation over the wave vectors to domain S lying between the circles of radius k_{min} and k_{max}:

$$\mathbf{E}(\mathbf{r}, t) = -\alpha \sum_{\substack{\mathbf{q} \\ q \in S}} \frac{\mathbf{q}}{q^3} \cos(\mathbf{q} \cdot \mathbf{r} + \varphi_{\mathbf{q}} - \omega_0 t) \ ,$$

$$S = \{ \mathbf{q} : k_{min}^2 \le q^2 \le k_{max}^2 \} \ ,$$

(25)

with $\alpha = -(a/L)(2\pi/L^2)$. On the contrary, taking the limit $L \to \infty$ cannot be done from the start: $\varphi_{\mathbf{q}}$ is not a regular function of $\mathbf{q}$, but a phase randomly chosen for every $\mathbf{q}$ between 0 and 2π. We must therefore derive the diffusion equation for a finite system, taking the limit $L \to \infty$ only at the end. The absolute diffusion equation

$$\frac{d \langle r^2(t) \rangle}{dt} = 2 \int_0^t d\tau C(\tau) = D(t)$$

(26)

(where $\langle \cdots \rangle$ represents an average over the random phase $\varphi_{\mathbf{q}}$) naturally introduces the "running" diffusion coefficient $D(t)$, also related to the velocity autocorrelation function

$$C(t) = \langle \mathbf{v}(t) \cdot \mathbf{v}(0) \rangle \ ,$$

where $\mathbf{v}(t)$ obeys the guiding-center equation of motion (1).

Following the method and making the approximations given in Ref. 16, one arrives at the following nonlinear

equation for absolute diffusion (valid for a finite square system of surface L^2):

$$\frac{d^2 \langle r^2(t) \rangle}{dt^2} \equiv 2C(t)$$

$$\equiv 2 \frac{c^2}{B^2} \sum_{\substack{\mathbf{k} \\ \mathbf{k} \in S}} \langle \mathbf{E}_{\mathbf{k}}(t) \cdot \mathbf{E}_{-\mathbf{k}}(0) \rangle e^{-1/4[k^2 \langle r^2(t) \rangle]}$$

(27)

to be compared with Eq. (14) in Ref. 16.

From the definition (25) of $\mathbf{E}(\mathbf{r}, t)$, it is very easy to compute the Fourier component $\mathbf{E}_{\mathbf{k}}(t)$ and therefore the correlation function

$$\langle \mathbf{E}_{\mathbf{k}}(t) \cdot \mathbf{E}_{-\mathbf{k}}(0) \rangle$$

$$= \left[\frac{\alpha}{2} \right]^2 \frac{1}{k^4} 2 \operatorname{Re}[e^{i\omega_0 t}(1 + \langle e^{-i\varphi_{\mathbf{k}}} e^{-i\varphi_{-\mathbf{k}}} \rangle)] \ . \quad (28)$$

Averaging over the random phases, we obtain

$$\langle \mathbf{E}_{\mathbf{k}}(t) \cdot \mathbf{E}_{-\mathbf{k}}(0) \rangle = \frac{\alpha^2}{2} \frac{1}{k^4} \cos \omega_0 t \ .$$

(29)

Substituting this result into Eq. (27) and using the relations and definitions corresponding to Eqs. (9)–(11), i.e.,

$$\alpha^2 = \frac{\langle | \mathbf{E}(\mathbf{r}, t) |^2 \rangle}{\sigma^2} = \frac{\tilde{E}^2}{\sigma^2} \ ,$$

(30)

with

$$\sigma^2 = \frac{1}{2} \sum_{\substack{\mathbf{k} \\ \mathbf{k} \in S}} \frac{1}{k^4} \ ,$$

(31)

we arrive at

$$\frac{d^2 \langle r^2(t) \rangle}{dt^2} = a^2 \cos(\omega_0 t) \frac{1}{\sigma^2} \sum_{\substack{\mathbf{k} \\ \mathbf{k} \in S}} \frac{1}{k^4} e^{-1/4[k^2 \langle r^2(t) \rangle]} \ ,$$

(32)

where we introduced

$$a = c \frac{\tilde{E}}{B}$$

as the amplitude of turbulence (note that this definition of a coincides with the drift velocity v_d introduced at the end of Sec. II). Note that, to avoid possible ambiguities, we derived the diffusion equation without any reference to a particular system of units.

As all quantities appearing in Eq. (32) remain well behaved in the limit of an infinite system, we may let L go to infinity. A little algebra then leads to the final differential equation

$$\frac{d^2 \Gamma(t)}{dt^2} = \frac{a^2 k_{min}^2}{2(1 - v^2)} \cos(\omega_0 t) [E_2(\Gamma) - v^2 E_2(\Gamma / v^2)]$$

$$\equiv F(t)$$

(33)

for the dimensionless function $\Gamma(t) = (\frac{1}{4}) k_{min}^2 \langle r^2(t) \rangle$; in

this equation v is equal to $k_{\min}/k_{\max}$ and $E_2(x)$ is the exponential integral function of order 2. Finally, note that this equation should be solved with the initial conditions $\Gamma(0)=\Gamma'(0)=0$.

Once this equation has been solved, the diffusion coefficient can be obtained by integrating the right-hand side [see Eq. (26)], which yields

$$D(t)=\frac{4}{k_{\min}^2}\int_0^t d\tau\, F(\tau)\ . \tag{34}$$

The latter two equations have a rather remarkable property: if, among the various models with different values of $k_{\min}$ and $k_{\max}$, we decide to examine one class, where $k_{\min}$ varies but v is kept constant, then this class is described by a single "scaled" solution. Indeed, if we introduce the "scaled" variables $\bar{a}=ak_{\min}$ and $\bar{D}=Dk_{\min}^2$, the equations above become

$$\frac{d^2\Gamma}{dt^2}=\frac{\bar{a}^2}{2(1-v^2)}\cos(\omega_0 t)[E_2(\Gamma)-v^2E_2(\Gamma/v^2)]\equiv F(t)\ ,$$
$$\bar{D}(t)=4\int_0^t d\tau\, F(\tau)\ . \tag{35}$$

In fact, even if the values of v for two models are not the same, this scaling property will still be nearly correct, since v is generally considered to be in the range $\frac{1}{25}<v<\frac{1}{12}$, and when v varies in this domain, the solution of the scaled equation changes by less than 1%. Note that this "approximate scaling" exists because we chose $k_{\min}$ and v and the field parameters, instead of $k_{\min}$ and $k_{\max}$, or $k_{\max}$ and v.

Up to now, any equation we wrote or any assertion we made was very general, since—as already noted—we did not choose any particular units system: we only dealt with physical quantities, not with their measures. However, when we want to compare the theoretical results to those of "computer experiments," we must make the nontrivial choice of units (here essentially of length and time). That this choice is nontrivial is, of course, due to the fact that, to give a precise physical meaning to any mathematical model, we must complete it with the "rules of the game," i.e., a system of units.

In computer simulations the units are always chosen so as to simplify the calculations, i.e., to eliminate as much as possible the parameters of the problem. Thus we chose, so to speak, $L=1$ and $\omega_0=2\pi$. This led us to the equation of motion (12), with the following form of the amplitude:

$$\mathcal{A}=\frac{2\pi}{\omega_0}\frac{1}{L}a\equiv\frac{2\pi}{\omega_0}c\frac{\tilde{E}}{B}\ .$$

However, if we want to compare our results (in particular, the variation of the diffusion coefficient in terms of the amplitude) with the theoretical predictions, we see at once that this choice is meaningless, since the theory is developed in the limit $L\rightarrow\infty$. It is then clear that our unit of length must be one of those that characterize the spectrum. To determine our choice, we now argue that we want it to lead to the "scaled" form (35) of the theoretical equations, i.e., that $k_{\min}$ must be absorbed in the amplitude. We therefore choose $\omega_0=2\pi$ as before

and $k_{\min}=2\pi$ (i.e., $\lambda_{\max}=2\pi$) or $t=2\pi\bar{t}/\omega_0$ and $l=2\pi\bar{l}/k_{\min}$, so that the theoretical equations for $\bar{\Gamma}(\bar{t})=\Gamma(t)$ and $\mathbb{D}(\bar{t})=D(t)k_{\min}^2/(2\pi\omega_0)$ now take the dimensionless form

$$\frac{d^2\bar{\Gamma}(\bar{t})}{d\bar{t}^2}=\frac{2\pi^2A^2}{1-v^2}\cos(2\pi\bar{t})[E_2(\bar{\Gamma})-v^2E_2(\bar{\Gamma}/v^2)]\equiv\bar{F}(\bar{t})\ ,$$
$$\mathbb{D}(\bar{t})=\frac{1}{\pi^2}\int_0^{\bar{t}}d\bar{\tau}\,\bar{F}(\bar{\tau})\ , \tag{36}$$

where the amplitude is

$$A=\frac{k_{\min}}{\omega_0}a\equiv\frac{k_{\min}}{\omega_0}c\frac{\tilde{E}}{B}\ .$$

The numerical solutions of Eqs. (36) is easily obtained and the resulting curve for $\ln\mathbb{D}$ versus $\ln A$ is shown on Fig. 15. The striking feature of this curve is that, outside the transition domain (i.e., $-1\lesssim\ln A\lesssim 1$), $\ln\mathbb{D}$ rapidly tends to limiting asymptotes with slopes equal to $+2$ for $\ln A\rightarrow-\infty$ and $+1$ for $\ln A\rightarrow\infty$.

At first sight, the $\mathbb{D}\sim A^2$ scaling may seem identical to the prediction of the quasilinear theory. In fact, this is not correct because, in the models we have considered, the electric field oscillates at one given frequency and a crude application of the quasilinear approximation would lead to a "diffusion coefficient" oscillating in time around a zero average. Thus, the nonlinear damping in our theoretical equation is here seen to be necessary to obtain the classical $D\sim A^2$ scaling.

In the asymptotic limit $A\rightarrow\infty$, the linear scaling $D\sim A$ may be understood at once as a Bohm (or frozen turbulence) scaling. Indeed, in this limit, the oscillating cosine factor may be forgotten in Eq. (36) which can then be integrated once to yield the following expression for the diffusion coefficient:

$$\mathbb{D}(\bar{t})=\frac{2A}{\pi}\left[\frac{1}{1-v^2}[\mathbb{F}(0)-\mathbb{F}(\bar{t})]\right]^{1/2}\ , \tag{37}$$

where

$$\mathbb{F}(\bar{t})=E_3[\bar{\Gamma}(\bar{t})]-v^4E_3[\bar{\Gamma}(\bar{t})/v^2]\ .$$

For long times, we thus find

$$\mathbb{D}(\bar{t}\rightarrow\infty)\rightarrow\frac{A}{\pi}\{2+2v^2\}^{1/2}\ . \tag{38}$$

Figure 15 also shows the "computer experimental" results we have obtained for models I and II. At first glance, the comparison between the theory and both models may lead to the following concise conclusions: (a) qualitatively, the agreement is good; (b) quantitatively, it is not too bad. Indeed, it is seen that model I as well as model II seem to exhibit both scalings predicted by the theory, and this is quite an encouraging result.

Quantitatively, the simulation points lie below the theoretical curve. But this cannot be a surprise, since both models lack important properties which are assumptions of the theory: in particular, the model systems are finite and therefore the wave-number spectrum is discrete; in addition, both models are anisotropic. That these facts may be important is suggested by the remark

that model II, which is closer to the theory, has the denser wave-number spectrum and is less anisotropic than model I.

Finally, we want to mention that non-Gaussian dynamics and intermittency can play an essential role in reducing the diffusion coefficient (without altering the classical $\langle r^2 \rangle \sim t$ diffusion law, see, for instance, Ref. 30. Non-negligible deviations from Gaussianity have been found in the stochastic dynamics of both models I and II. Moreover, non-Gaussianity is an important property of the dynamics of real turbulent fluids and plasmas. As an example, strong marks of non-Gaussian behavior in the dynamics of density fluctuations have been recently observed in tokamak TFR (Ref. 31) and in tokamak AS-DEX (Ref. 32). These deviations from Gaussian statistics are not taken into account in the theory which is based on a quasinormal approximation.

B. Relative diffusion

The relative diffusion equation for the mean-square relative distance $\langle \delta r^2(t) \rangle$ between two particles is given by the equation[16]

$$\frac{d\langle \delta r^2(t) \rangle}{dt} = 2\int_0^t d\tau \langle \mathbf{g}(t) \cdot \mathbf{g}(t-\tau) \rangle$$

$$= 2\langle g^2(t) \rangle \int_0^t d\tau R_{12}(\tau,t) \tag{39}$$

in terms of the autocorrelation of relative velocity

$(\mathbf{g} = \mathbf{v}_1 - \mathbf{v}_2)$ or of the normalized autocorrelation

$$R_{12}(\tau,t) = \frac{\langle \mathbf{g}(t) \cdot \mathbf{g}(t-\tau) \rangle}{\langle g^2(t) \rangle} . \tag{40}$$

The theory is based on a separate analysis of the two factors in the right-hand side of Eq. (39). First, a very simple model is used to represent the τ dependence of the relative velocity autocorrelation. It has been established that the microscopic Lagrangian correlation time (which characterizes this τ dependence) is actually related to the value of the absolute diffusion coefficient. The result obtained for relative diffusion is thus given in terms of one constant, the diffusion coefficient, described in the preceding paragraph. In the present paper, we deal with the so-called model "a" of Ref. 16, or the "constant Lagrangian model," where the correlation time τ_c is assumed to be constant in time, and

$$R_{12}(\tau,t) = e^{-\tau/\tau_c} . \tag{41}$$

On the other hand, nonlinear dependence of $\langle g^2(t) \rangle$ on the amplitude of turbulence has been shown to be responsible for the clump effect, i.e., a strong decrease of relative diffusion of a small cloud of particles, followed by an exponential separation of the trajectories. The nonlinear description of $\langle g^2(t) \rangle$ is based on the Corssin factorization assumption, and on the Weinstock "second-cumulant approximation" which is a Gaussian-like hypothesis. An important goal in the present numerical
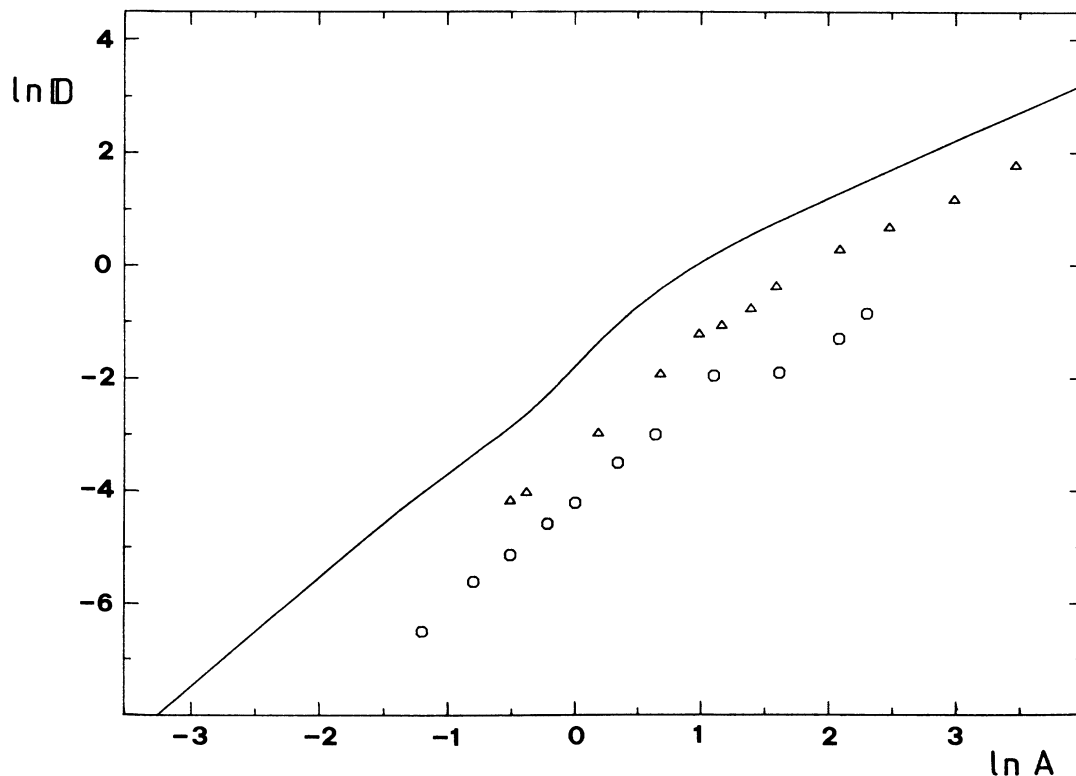
FIG. 15. Comparison of the results for $D(A)$ vs A. Solid line represents the theoretical results from Eq. (36) for both $\nu = \frac{1}{12}$ and $\nu = \frac{1}{25}$. Circles refer to model I and triangles to model II.

simulation consists in testing the validity of these approximations.

The time dependence of the relative diffusion can be described by the dimensionless function

$$Z(t) = \tfrac{1}{4} k_{\min}^2 \langle \delta r^2(t) \rangle ,$$

(42)

which obeys the following nonlinear equation (from this point and unless otherwise stated, we adopt the system of units introduced in the preceding section, where $\omega_0 = 2\pi$ and $k_{\min} = 2\pi$; moreover, to be as clear as possible we drop the overbar of $\bar{t}$, etc.):

$$\frac{dZ}{dt} = 4\pi^2 A^2 t_R(t) \left[1 - \frac{1}{1-v^2} [E_2(Z) - v^2 E_2(Z/v^2)] \right] ,$$

(43)

where the Lagrangian time scale $t_R(t)$ depends on the model considered for the autocorrelation function

$$t_R(t) = \int_0^t d\tau \, R_{12}(\tau, t) .$$

(44)

We introduce a timelike variable Θ defined by

$$\frac{d\Theta(t)}{dt} = 4\pi^2 A^2 t_R(t), \quad \Theta(0) = 0$$

(45)

which allows us to split the problem into two parts:[16] (i)

the description of $Z(\Theta)$ given by

$$\frac{dZ}{d\Theta} = 1 - \frac{1}{1-v^2} [E_2(Z) - v^2 E_2(Z/v^2)] ;$$

(46)

(ii) the t dependence of the variable $\Theta(t)$, which depends on the model considered, here the constant Lagrangian memory model with R_{12} given by Eq. (39). In this model one obtains

$$\frac{d\Theta}{d\tilde{t}} = \tilde{\tau}_c \left[1 - \exp \left[-\frac{\tilde{t}}{\tilde{\tau}_c} \right] \right] ,$$

(47)

where we have introduced a new time variable $\tilde{t} = 2\pi At$. The explicit form of $\tilde{\tau}_c$ is given in Ref. 12 and becomes in our unit system $\tilde{\tau}_c = \pi \mathbb{D}/A$. The results for $Z(t)$ turn out to be naturally expressed in terms of the scaled time $t_d = \tilde{\tau}_c \tilde{t} = 2\pi^2 \mathbb{D}t$. Here we present the results obtained with the initial value $\log Z_0 = -5.608$ which corresponds to the initial separation of particles adopted in numerical simulations of model I.

In the range of values of A from 0.45 to 1.90 the curves $Z(t_d)$ calculated from Eqs. (46) and (47) for the corresponding values of the diffusion coefficient (as given by the simulation) appear to be indistinguishable from each other. They are represented by the continuous curve on Fig. 16, where one observes that after a very slow initial
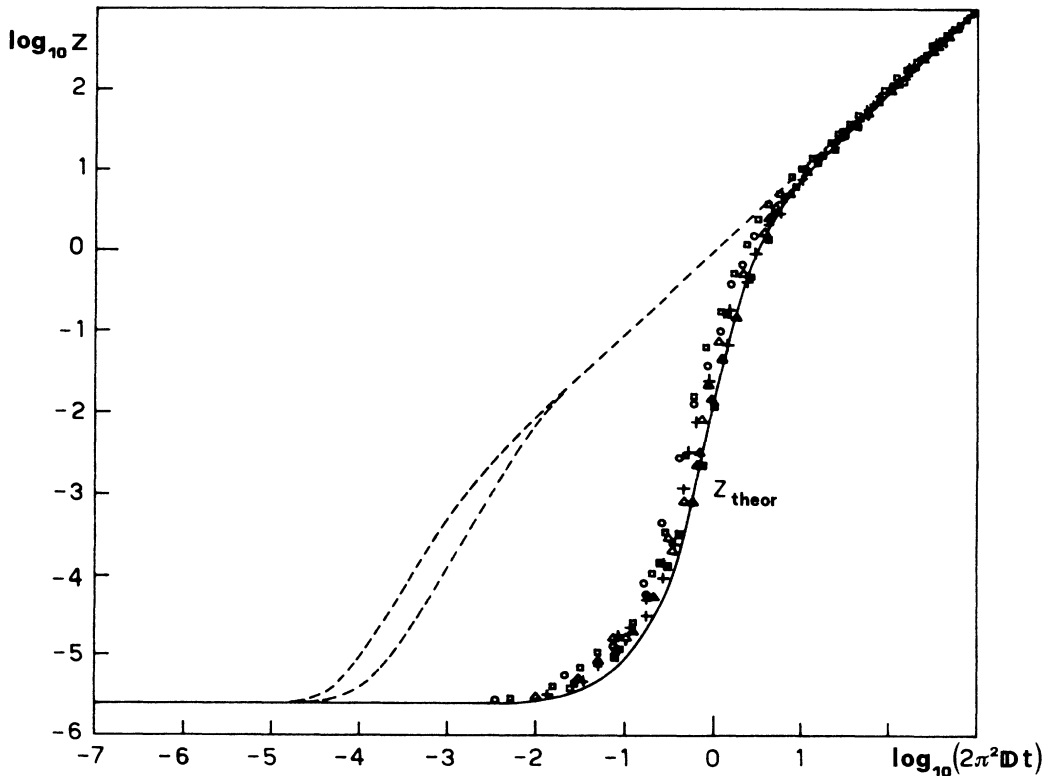
FIG. 16. The solid curve (several superposed curves) is the theoretical prediction for relative diffusion when A varies between 0.45 and 1.90. The dashed curves are the predictions without clump effect at $A = 0.45$ and 1.90. The various points are simulation results for model I (for A varying in the same range). To compare with Fig. 8, note that here decimal logarithms are used.

growth, a rapid exponential behavior takes place, towards a final stage where Z behaves as t_d, as expected. In order to visualize the clump effect, we have also represented in dashed lines, for the two extreme cases $A = 0.45$ and 1.90, the uncorrelated results which are obtained by neglecting the nonlinear effects of trajectory correlations, i.e., the second term in the right-hand side of Eq. (46). It appears that the time behavior obtained in the numerical simulation (Fig. 16) actually follows rather precisely the continuous theoretical curve. This important result constitutes a very positive indication of the accuracy of the approximations used in order to take the nonlinearity into account in the theoretical description. Moreover, the function $\langle \delta r^2(t) \rangle$, when plotted versus t_d, appears to be nearly insensitive to the exact value of the absolute diffusion coefficient $\mathbb{D}$ over a wide range of values (for $\mathbb{D} = 10^{-3}$ to 10^{-1}; see Eq. (19).

For higher amplitudes of turbulence ($\mathbb{D} \sim 1$) a displacement of the curve is predicted towards larger times. In other words, the "universal" curve [Eq. (19)] obtained in the numerical simulation is not expected to hold for large values of $\mathbb{D}$ and A.

We now discuss the analytical prediction for the relative diffusion of nearby trajectories on the basis of Eqs. (46) and (47). For sufficiently small initial separation, such that $Z(0) \ll v^2/2$, a time regime appears in which the solution is given by

$$Z(\Theta) = Z(0)\exp(2\chi\Theta) , \qquad (48)$$

where χ is a positive Lyapunov exponent, given by

$$2\chi = \mathbb{K}_0^2/k_{\min}^2 = \frac{\ln v^2}{v^2 - 1}$$

[$\mathbb{K}_0$ is the r.m.s. value of the wave vector $\mathbf{k}$, weighted by the corresponding $S(\mathbf{k}) \sim k^{-4}$]. This exponential growth of the separation with growing Θ is also an exponential growth in time, since $\Theta \sim \tilde{\tau}_c \tilde{t}$ for small value of $\tilde{\tau}_c$, and hence for $\mathbb{D}$ and A vanishing.

The argument in Eq. (48) is then $2\chi\Theta = 2\chi\tilde{\tau}_c\tilde{t}$ $= 4\pi^2\chi\mathbb{D}t = 2\lambda t$ thus defining the characteristic exponent

$$\lambda = 2\pi^2\chi\mathbb{D} = \pi^2\frac{\ln v^2}{v^2 - 1}\mathbb{D} \sim A^2 . \qquad (49)$$

This law, predicted for small values of A, is actually verified qualitatively in the simulation of model I (see Fig. 9) up to $A \sim 0.5$. The quantitative agreement is not very precise: for $A = 0.3$, for instance, where $\mathbb{D} \sim 0.002$, the simulation gives $\langle h \rangle \simeq 0.09 \approx \lambda$, while the prediction (49) gives $\lambda = 0.13$. However, this is not surprising because the quantity χ defined in Eq. (48) is not exactly equal to $\langle h \rangle$. The difference between $\langle h \rangle$ and χ could be due to intermittency effects.[33] Following the definitions of generalized Lyapunov exponents given in Ref. 33, $\langle h \rangle$ corresponds to $dL(q)/dq \mid_{q=0}$ and χ to $L(2)/2$, and in general one has $\chi > \langle h \rangle$.

VII. CONCLUSIONS

In order to study the diffusion of charged particles across a strong magnetic field, due to a known spectrum of electrostatic turbulence, we have investigated the dynamical behavior of two different nonlinear Hamiltonian systems. The electron dynamics is described in the guiding-center approximation. The guiding-center equation of motion is a nonautonomous Hamiltonian system of 1.5 degrees of freedom whose phase space is the two-dimensional physical space (perpendicular to magnetic field). The Hamiltonian is formally proportional to the electrostatic potential.

A turbulent electrostatic potential is simulated by superposing several hundreds of propagating waves with random spatial phase shifts. The amplitudes of these waves are such as to yield a k^{-3} energy spectrum (within two extrema $k_{\min}$ and $k_{\max}$) in analogy with the observed features of electrostatic turbulence in tokamaks. The difference between the two models lies in the summation domain in wave-number space. The equation of motion has been solved numerically.

An important property of these models is that when the average electric field amplitude is large enough, "most" trajectories become chaotic at large scale (i.e., the phase space has an unbounded and connected stochastic component) and diffusion across magnetic field sets in. Following several hundreds of particles trajectories, an analysis of the statistical properties of this chaotic dynamics has been performed: we studied the absolute diffusion, the relative diffusion of neighboring particles, the Kolmogorov-Sinai entropy, and other quantities measuring the deviation from Gaussian statistics (kurtosis of the distribution of absolute and relative displacements, kurtosis of the velocity distribution, velocity autocorrelation functions).

The main result found for absolute diffusion concerns the existence of two scaling regimes of the diffusion coefficient D with the average electric field amplitude A. D scales as A^2 at low amplitudes and as A at high amplitudes. This shows that simple and low-dimensional dynamical models can be (at least) in qualitative agreement with existing theories. In fact, these two regimes can be identified with the quasilinear and Bohm scalings, respectively. This is a relevant difference with more simplified models where slower dependences of D versus A were found.

As for relative diffusion, we have observed the so-called clump effect; moreover, the relative diffusion curve has been shown to satisfy a scaling law in the domain of moderate values of A: the curves obtained at different A superpose when plotted versus a time variable scaled with the absolute diffusion coefficient D. Two different models have been used to test the "structural stability" of the results: a satisfactory agreement has been obtained.

The numerical results have been compared with a recently proposed theoretical treatment of the turbulent diffusion of guiding centers. The theory has been adapted to be compared with the numerical simulations; it yields the quasilinear and Bohm scalings as limiting regimes with a transition between them.

A good qualitative agreement has been found between theory and simulation. However, there is a systematic deviation between the theoretical and numerical values of the diffusion coefficients. This discrepancy could be attri-

buted to the fact that the theoretical values of the diffusion coefficient have been obtained in the continuum limit $(L \rightarrow \infty)$, for an isotropic turbulent electric field and using a quasinormal approximation. These assumptions have not been taken into account by the numerical models; on the other hand, in view of a comparison among theory, numerical simulations, and real physical situations, it is doubtful, for instance, whether a Gaussian model is the best for representing the real physics of tokamaks.

A very good agreement between theory and simulation has been found for the time dependence of relative diffusion of pairs of initially close particles. Both theory and simulation agree on the existence of a scaling law for relative diffusion, at least in the domain of moderate values of the amplitude of turbulence. Finally, a good agreement between theory and simulation has been found at small A for the Lyapunov exponents.

ACKNOWLEDGEMENTS

[1]L. A. Artsimovich, Nucl. Fusion **12**, 215 (1972); H. P. Furth, *ibid*. **15**, 487 (1975).

[2]P. C. Liewer, Nucl. Fusion **25**, 543 (1985).

[3]E. Mazzuccato, Phys. Rev. Lett. **36**, 792 (1976); for the subsequent references on this point see Ref. 2.

[4]TFR Group and A. Truc, Plasma Phys. Contr. Fusion **26**, 1045 (1984).

[5]G. Becker *et al.*, Nucl. Fusion **23**, 1293 (1983); M. Keilhacker *et al.*, Plasma Phys. Contr. Fusion **26**, 49 (1984).

[6]B. B. Kadomtsev, *Plasma Turbulence* (Academic, London, 1965); R. Z. Sagdeev and A. A. Galeev, *Nonlinear Plasma Theory* (Benjamin, New York, 1969).

[7]T. H. Dupree, Phys. Fluids **9**, 1773 (1966); **10**, 1049 (1967).

[8]J. Weinstock, Phys. Fluids **12**, 1045 (1969); J. H. Misguich and R. Balescu, J. Plasma Phys. **13**, 385 (1978); Plasma Phys. **24**, 284 (1982).

[9]R. H. Kraichnan, Phys. Fluids **10**, 1417 (1967).

[10]T. H. Dupree, Phys. Fluids **15**, 334 (1972).

[11]B. B. Kadomtsev and O. P. Pogutse, Phys. Fluids **14**, 2470 (1971).

[12]J. H. Misguich and R. Balescu, Plasma Phys. **24**, 284 (1982).

[13]R. Balescu and J. H. Misguich, in *Statistical Physics & Chaos in Fusion Plasma*, edited by C. W. Horton and L. E. Reichl (Wiley, New York, 1984), p. 295.

[14]R. G. Kleva and J. F. Drake, Phys. Fluids **27**, 1686 (1984).

[15]W. Horton, Plasma Phys. Contr. Fusion **27**, 937 (1985).

[16]J. H. Misguich, R. Balescu, H. L. Pécseli, T. Mikkelsen, S. E. Larsen, and Qiu Xiaoming, Plasma Phys. Contr. Fusion **29**, 825 (1987).

[17]M. Pettini, A. Vulpiani, J. H. Misguich, R. Balescu, M. De Leener, and J. Orban, EURATOM-CEA-FC (Commisssariat à L'Energie Atomique-Fusion Contrôlée) Report No. 1271, 1986 (unpublished).

[18]M. Hénon, C. R. Acad. Sci. Ser. A **262**, 312 (1966).

[19]A. J. Lichtenberg and M. A. Lieberman, *Regular and Stochastic Motion* (Springer-Verlag, New York, 1983).

[20]G. Benettin, L. Galgani, and J. M. Strelcyn, Phys. Rev. A **14**, 2338 (1976).

[21]G. Contopoulos, L. Galgani, and A. Giorgilli, Phys. Rev. A **18**, 1183 (1978); M. Pettini and A. Vulpiani, Phys. Lett. A **106**, 207 (1984).

[22]Our range of values of A is too small to conclude that $\langle h \rangle \sim \ln A$, but this provides a good fit.

[23]J. L. Tennyson, J. R. Cary, and D. F. Escande, Phys. Rev. Lett. **56**, 2117 (1986); J. R. Cary, D. F. Escande, and J. L. Tennyson, Phys. Rev. A **34**, 4256 (1986).

[24]M. Suzuki, Progr. Teor. Phys. **71**, 67 (1984).

[25]F. De Pasquale, P. Tartaglia, and P. Tombesi, Phys. Lett. A **72**, 7 (1979); Z. Phys. B **43**, 353 (1981).

[26]D. F. Escande, Phys. Rep. **121**, 163 (1985).

[27]A. S. Monin and A. M. Yaglom, *Statistical Fluid Mechanics: Mechanics of Turbulence* (MIT Press, Cambridge, 1975), Vol. 2.

[28]T. Geisel, Europhys. News **15**, 5 (1984); T. Geisel and J. Nierwetberg, Phys. Rev. Lett. **48**, 7 (1982); Phys. Rev. A **29**, 2304 (1984); E. Marinari, G. Parisi, D. Ruelle, and P. Windey, Commun. Math. Phys. **89**, 1 (1983).

[29]V. Merlo, M. Pettini, and A. Vulpiani, Nuovo Cimento Lett. **44**, 163 (1985).

[30]U. Balucani, V. Tognetti, R. Vallauri, P. Grigolini, and P. Marin, Z. Phys. B **49**, 181 (1982); U. Balucani, V. Tognetti, R. Vallauri, P. Grigolini, and M. P. Lombardo, Phys. Lett. A **86**, 426 (1981).

[31]H. J. Barkley, J. Andreoletti, F. Gervais, J. Olivain, A. Quemeneur, and A. Truc, EURATOM-CEA-FC Report No. 1294, 1986 (unpublished); Plasma Phys. Contr. Fusion **30**, 217 (1988).

[32]L. Battiston *et al.*, *Dimensionality of Fluctuations in ASDEX (Axial Symmetric Divertor Experiment), Contributed Papers of the Thirteenth European Conference on Controlled Fusion and Plasma Heating, Schliersee, FRG, 1986*, edited by G. Brifford and M. Kaufman (European Physical Society, Schliersee, 1986), Europen Conference Abstracts, Vol. 10, Pt. I, p. 81.

[33]R. Benzi, G. Paladin, G. Parisi, and A. Vulpiani, J. Phys. A **18**, 2157 (1985).
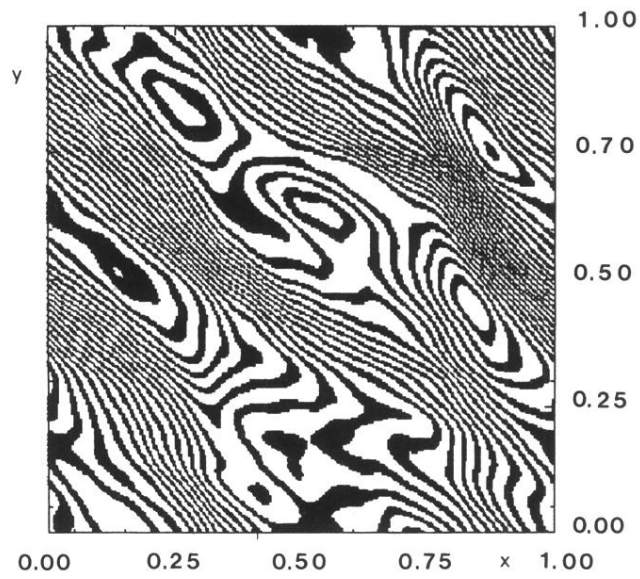
FIG. 1. Equipotential curves [Eq. (5)] of the turbulent electric field (for $t = 0$). The thickness of lines is proportional to the local flatness of the potential.
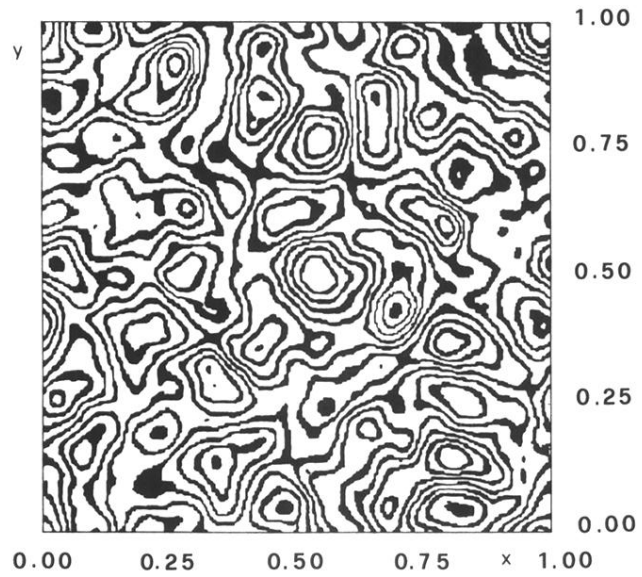
FIG. 13. Equipotential curves for the turbulent field in model II at $t = 0$ [from Eq. (23)]. A more isotropic field structure shows up.

FIG. 5. Stroboscopic sections for (a) $A = 0.45$ (QL region),
$x_0 = 0.741$, $y_0 = 0.749$ (3000 points); (b) $A = 5.0$ (Bohm region),
$x_0 = 0.741$, $y_0 = 0.749$ (9000 points).